Available online at www.sciencedirect.com
ScienceDirect
Computers and Structures 85 (2007) 1808–1827
Computers & Structures
www.elsevier.com/locate/compstruc

Region-by-region modeling of laminated composite plates

P.M. Mohite, C.S. Upadhyay *

Department of Aerospace Engineering, Indian Institute of Technology, Kanpur 208016, India

Received 17 May 2006; accepted 4 April 2007
Available online 30 May 2007

Abstract

Several plate models have been proposed in the literature for the analysis of laminated plates. These are based either on an equivalent through-thickness formulation or a layerwise formulation. It is shown in the literature that while the equivalent models are economical, the layerwise models are expensive but are also more accurate, especially with respect to the transverse stresses. Generally, the same model is used throughout the domain. The current study addresses the issue of economical and accurate computation of local stresses, strains and displacements (as well as global quantities) using combinations of layerwise, equivalent or intermediate models in various regions of the domain. A region-by-region modeling strategy is presented for a chosen general family of equivalent, intermediate and layerwise models. The proposed strategy allows the user to put any model (of any order in the thickness direction) in any desired region of interest. The effectiveness of the strategy is demonstrated through numerical examples. It is shown that this approach can significantly reduce computational cost and can also lead to good resolution of the local stress and displacement fields for domains with unsymmetric laminae, cut-outs, local damage, corner edges, sudden transition of boundary conditions and material.

Keywords: Composite laminates; Plate models; Layerwise; Equivalent; Region-by-region; Transverse deflection; Equilibrium approach

1. Introduction

Laminated structures are generally thin, and thus several dimensionally reduced models (or reduced 2D models) have been proposed in the literature for the study of these structures. These models (popularly known as plate models) are based on either displacement based (see [1–4]) or mixed formulations (see [5–8]). A comparison of these models can be seen in [7]. An excellent review of various types of plate models (especially the layerwise and zig-zag models) has been given in [9]. The plate models are classified according to the through-thickness representation of the displacement field [1–4], transverse shear strain/stress field (for mixed formulation based elements [5] and references therein) and the interlaminar continuity conditions imposed (for layerwise models [10]).

In this study, we will focus on plate models based on the displacement formulation. These models can be categorized as:

(1) Shear deformable theories (see [3,4]).
(2) Zig-zag theories (see [1,2,9] and references therein).
(3) Layerwise theories (see [11–17]).

For the families of models given above, the attractive feature is that the models are independent of the number of layers, i.e. the computational cost does not depend on the number of layers. Some of the zig-zag models have also shown to be convergent to the three-dimensional elasticity solution with respect to the strain energy (energy norm). These models focus on representing the transverse shear effects more accurately, by enriching the representation field in the z-direction. Another important issue has been that of shear locking in the case of thin plates. Several "locking free" shear deformable models have been proposed in the literature (see [3,4]).

* Corresponding author. Tel.: +91 512 2597936; fax: +91 512 2597561.
E-mail address: shekhar@iitk.ac.in (C.S. Upadhyay).

0045-7949/$ - see front matter © 2007 Elsevier Ltd. All rights reserved.
doi:10.1016/j.compstruc.2007.04.005

A major drawback with these models has been that the transverse stresses, obtained using these models, are not accurate. An equilibrium based postprocessing approach can be (see [11–13]) used to extract the transverse stress components accurately. This approach is quite effective in most cases. However, for domains with unsymmetry in layup, existing delamination and ply level damage, the dimensionally reduced models are ineffective. In order to handle these problems a more refined analysis is desired. Layerwise models (see [6,11,13,14] and references therein, [15,18–20]) and intermediate models are often used to resolve this issue. In the layerwise models, the standard plate models are applied layerwise (see [16,17]), and continuity of displacement (and transverse shear stresses in some cases [10]) is imposed at the interlaminar interfaces. The intermediate model is based on using the dimensionally reduced models piecewise (i.e. lump all laminae above and below a delamination separately). The use of these models leads to enhanced resolution of the local effects, but it also increases the size of the problem to be solved. In [13,15], a generalized layerwise model is given which is based on use of one-dimensional hierarchic basis functions in the transverse and the planar directions. These models allow for use of different approximation orders in the transverse and planar directions. Thus, the transverse order of approximation can be raised for each layer. These models are essentially three-dimensional models and have been shown to be very accurate with respect to any pointwise quantity of interest. An exhaustive review of the existing literature, on laminated plate and shell models, can be seen in [21].

Generally, the strong three-dimensional effects are localized (see [22–27]) in the vicinity of boundaries (boundary layer), vertices (vertex singularities), edges (edge and vertex edge singularities), parts of lamina/laminae (damaged lamina) and local interfaces (interlaminar delamination). An example of such a situation is shown in Fig. 1. In these cases, beyond a local neighborhood of the regions of unsmooth behavior (in the vicinity of damaged zone boundaries), the solution can be effectively represented using any of the families of dimensionally reduced models. Hence, the approximation is required to be enriched only in the regions where the solution is not smooth. To achieve this, here we propose a region-by-region solution approach. The goal has been to give a generalized, computationally implementable, procedure to incorporate models of any complexity in any region of interest. It will be shown that this approach leads to tremendous savings in computational cost and gives accurate representation of the state of stress, strain and displacement, in the region of interest. This approach is a generalization of the planar constrained approximation approach of [32] and the *h–d* approach of [33], given for homogeneous materials. In this study, we do not address the issue of adaptivity for control of modeling and discretization errors. Estimation and control of discretization error has been discussed in [11,12]. However, note that the current approach is naturally amenable to an adaptive analysis. Estimation and control of modeling error will be discussed in a forthcoming paper.

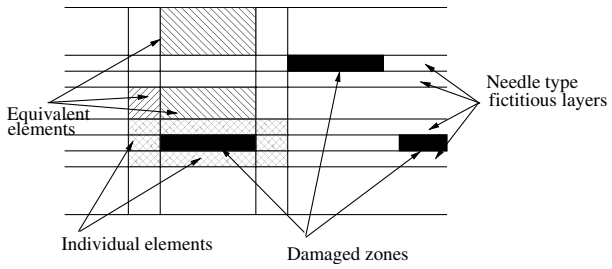

Fig. 1. Cross-sectional representation of a generic laminated structure with damaged regions. The generic modeling strategies with equivalent, intermediate, layerwise and sublaminae based modeling is also depicted.

Note that several approaches have been proposed in the literature (for different classes of problems), using the global–local solution procedure. Examples of such procedures are the Arlequin method [28], the overlapping grid method [29] (also known as chimera method used in fluid mechanics) and global–local method [30]. In these methods either the global solution is used as the boundary condition for a more refined local analysis, or various models are glued together (weakly) through some edge constraint or penalty conditions. Following [31], these approaches are useful when the solution is smooth everywhere and the far-field influence on the local approximate solution is not significant (see [31] for details).

2. Plate models

Analysis of thin laminated structures is based on using predefined transverse functions in the z-direction, with the displacement field given as a series in terms of products of the transverse functions and planar functions. Various families of plate models can be defined based on the specific definitions of the transverse functions. The particular plate models employed in this study belong to the families of plate models given below.

2.1. Equivalent models (EQ)

These are conventionally the most popular plate models, with CLPT and HSDT models as special cases. The displacement fields corresponding to these models can be defined as

$$\{u\} = \begin{Bmatrix} u_1(x,y,z) \\ u_2(x,y,z) \\ u_3(x,y,z) \end{Bmatrix} = \begin{Bmatrix} \sum_{i=1}^{p_z^1+1} u_{1i}(x,y)\phi_i(z) \\ \sum_{i=1}^{p_z^2+1} u_{2i}(x,y)\psi_i(z) \\ \sum_{i=1}^{p_z^3+1} u_{3i}(x,y)\zeta_i(z) \end{Bmatrix} \tag{1}$$

Here, $p_z^i, i = 1,2,3$ is the order of the polynomial transverse functions in the z-direction for u_1, u_2 and u_3, respectively.

Generally $p_z^1 = p_z^2$ is chosen. Here, z is chosen with respect to the middle plane of the plate. Note that for isotropic plates and also for symmetric laminates subjected to transverse loads, $u_1(x,y,z)$ and $u_2(x,y,z)$ are antisymmetric, while $u_3(x,y,z)$ is symmetric with respect to z. Hence, following [34,38], $p_z^1 = p_z^2 = 1$ and $p_z^3 = 0$ is chosen as the first order shear deformable theory. This is represented as the $(1,1,0)$ model. The HSDT model is generally taken as $(3,3,0)$. The transverse functions are polynomials defined over the full thickness. Following [34], a natural hierarchy of such models is given by $(1,1,0)$, $(1,1,2)$, $(3,3,2)$, $(3,3,4)$, ... These models generally correspond to bending effect (i.e. plate under transverse loading). In the current study, both the conventional definition and the sequence of models due to [34] are used. Conventionally, the functions $\phi_i(z) = \psi_i(z) = \zeta_i(z)$ are taken as the monomials z^{i-1}. Here we have taken $\phi_i(z) = \psi_i(z) = \zeta_i(z) = M_i(\hat{z})$, where $M_i(\hat{z})$ is the Legendre polynomial based hierarchic shape function (see Fig. 2) defined in terms of $\hat{z} = \frac{2}{t}z$, where t is the total thickness of the plate. The functions are

$$M_1(\hat{z}) = \frac{1}{2}(1-\hat{z}); \quad M_2(\hat{z}) = \frac{1}{2}(1+\hat{z});$$
$$M_3(\hat{z}) = \frac{1}{2\sqrt{6}}(3\hat{z}^2 - 3); \quad M_4(\hat{z}) = \frac{1}{2\sqrt{10}}(5\hat{z}^3 - 5\hat{z});$$
$$M_5(\hat{z}) = \frac{1}{8\sqrt{14}}(35\hat{z}^4 - 42\hat{z}^2 + 7) \tag{2}$$

For isotropic plates and symmetric laminates, in-plane loads lead to in-plane or membrane stresses. In this case, u_1 and u_2 are symmetric with respect to z and u_3 is antisymmetric. Following [34], the sequence of models for this case is given by $(0,0,1)$, $(2,2,1)$, $(2,2,3)$, $(4,4,3)$, ... Note that for isotropic plates and symmetric laminates the bending and membrane effects are decoupled. However, for antisymmetric or unsymmetric laminates, both bending and membrane effects are coupled and hence $(1,1,1)$, $(2,2,2)$, $(3,3,3)$, ... models should be ideally used. However, for these laminates also, as is commonly used, we have employed the bending displacement representation when transverse loads are applied. The in-plane approximation order (for $u_{ij}(x,y)$) is the same for all the components and is denoted by p_{xy}. Members of this family of models will be represented by $\mathrm{EQ}p_{xy}p_z^1p_z^2p_z^3$. For example EQ3110 corresponds to the equivalent model with $p_{xy} = 3$ and $p_z^1, p_z^2 = 1, p_z^3 = 0$.

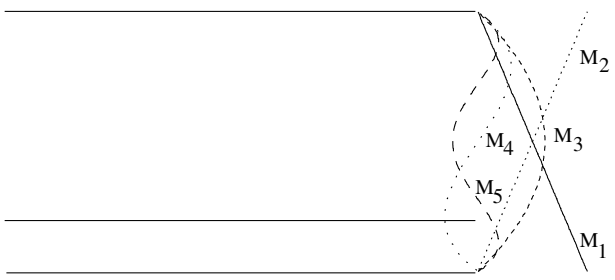

Fig. 2. Transverse approximation for equivalent model: example of fourth-order transverse approximation.

2.2. Intermediate models (IM)

Generally, the critical local quantities of interest are desired in particular lamina or at the interface of two laminae. Initiation of failure is one such quantity of interest. Further, analysis of initially damaged laminates with embedded lamina level damage or delaminations requires accurate representation of the local displacement, strain and stress state. In this case, the equivalent models cannot be used. The intermediate models are based on defining the transverse functions for a group of laminae and not the full laminate. From Fig. 3, it can be seen that the transverse functions are defined as the one-dimensional hierarchic basis functions $\overline{M}_i(z)$. The displacement field is defined, in terms of the functions $\overline{M}_i(z)$, as

$$u_1(x,y,z) = \sum_{i=1}^{n_1} u_{1i}(x,y)\overline{M}_i(z)$$
$$u_2(x,y,z) = \sum_{i=1}^{n_2} u_{2i}(x,y)\overline{M}_i(z) \tag{3}$$
$$u_3(x,y,z) = \sum_{i=1}^{n_3} u_{3i}(x,y)\overline{M}_i(z)$$

Generally, $n_1 = n_2$. Note that now n_1 and n_3 depend on the number of lamina groups in the thickness direction, with the order of the transverse functions taken to be the same in each group of laminae, given by p_z^1, p_z^2 and p_z^3. This leads to an increase in the number of transverse functions $\overline{M}_i(z)$ and hence the number of unknown functions $u_{ij}(x,y)$. Similar to the convention employed above, these models will be denoted by $\mathrm{IM}p_{xy}p_z^1p_z^2p_z^3$. Note that different orders of transverse functions can be used in each group of laminae, but have not been employed in this study.

2.3. Layerwise models (LM)

This is the most general three-dimensional representation of the displacement field. Each lamina is taken as a separate group and the transverse functions are defined as the one-dimensional basis functions defined over the lamina. From Fig. 4, it can be seen that the representation of the displacement field is given by

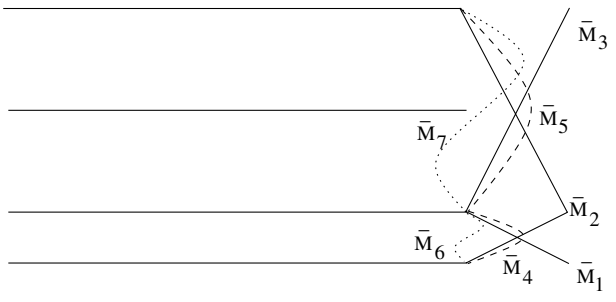

Fig. 3. Transverse approximation for intermediate model: example of cubic order transverse approximation.

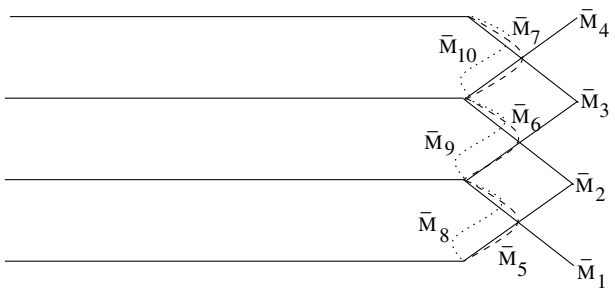

Fig. 4. Transverse approximations for layerwise model: example of cubic order transverse approximation.

$$u_1(x,y,z) = \sum_{i=1}^{n_1} u_{1i}(x,y)\overline{M}_i(z)$$
$$u_2(x,y,z) = \sum_{i=1}^{n_2} u_{2i}(x,y)\overline{M}_i(z) \quad (4)$$
$$u_3(x,y,z) = \sum_{i=1}^{n_3} u_{3i}(x,y)\overline{M}_i(z)$$

where $n_1 = n_2$ and n_3 depend on the order of approximation $p_z^1 = p_z^2$, p_z^3 and the number of laminae (or layers) nl in the laminate. Hence, here the number of unknowns grows with the number of laminae. Members of this family of models will be represented by $\mathrm{LM}p_{xy}p_z^1p_z^2p_z^3$.

3. Concept of sublaminae

For the intermediate and layerwise models, it is possible to partition a lamina into multiple laminae, with different thickness, as shown in Fig. 1. Hence, in the vicinity of delaminations, ply damage, resin rich regions, etc. the approximation can be suitably enriched by using a graded division of the lamina, leading to needle shaped elements (that is, elements with high aspect ratios) in the neighborhood of the flaws. This should lead to a more accurate representation of the state of stress in the vicinity of the flaws (see Fig. 1 for details). The approximation is now constructed using representation of (3) or (4), defined with the sublaminae assumed to be independent laminae. Note that the sublaminae are referred to as 'numerical sublayers' in the open literature. A similar approach was used in [33] for the Euler–Bernoulli beam model.

Remark 1. It has been shown in [26], that for such three-dimensional problems corner, corner edge and edge singularities may also exist. The sublaminae concept, along with graded refinements in the plane, can be used to effectively capture these singularities.

4. Region-by-region modeling (RR)

4.1. Motivation

In a structural component, the "hot-spots" are generally localized in the vicinity of structural details, boundaries of the domain (faces and edges), re-entrant corners, cut-outs, existing delaminations and ply-failure zones. The solution is unsmooth in the vicinity of these details, while it is very smooth in the remaining part of the domain (see Figs. 1 and 5). In order to get an accurate representation of the solution everywhere, it is desirable to use an enriched approximation model (LM or IM with sublaminae if desired) only in the vicinity of the "hot-spot", while in the rest of the domain, a lower order model will suffice. In this study, p_{xy} is uniform over the whole domain, while the approximation enrichment is done by using either a higher value of p_z^i and/or a more refined model, e.g. IM or LM. Thus it is important to build the capability to put any desired model in a specified region, rather than doing an overkill by using a higher model everywhere in the domain (which will be computationally very expensive for a laminate with many layers). This concept has been introduced through the region-by-region modeling approach described in this section.

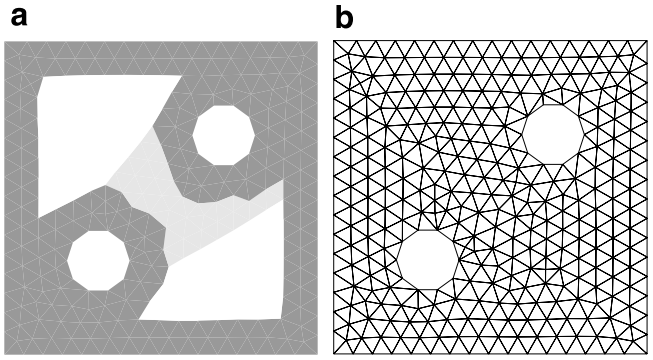

Fig. 5. Illustration of region-by-region model. (a) Division of domain into regions and (b) two-dimensional mesh over the domain.

4.2. Concept of regions

As an illustrative example, let us consider the domain given in Fig. 5, with the two circular cut-outs shown. In the vicinity of the cut-outs (free edge) and the outer boundaries of the domain (shown with grey shade in Fig. 5(a)), the solution is expected to be unsmooth, have severe boundary layer effect, and possibly be three-dimensional in nature. Hence along with a refinement of the mesh, enrichment of the model will also be desired in the shaded regions. Thus, the domain is divided into multiple regions (three regions shown by different shades of grey). The plate model is then fixed for each region. For example, for the domain of Fig. 5(a), $\mathrm{EQ}p_{xy}p_z^1p_z^2p_z^3$ may be used in the unshaded region; $\mathrm{IM}p_{xy}p_z^1p_z^2p_z^3$ may be used in the lighter grey region and $\mathrm{LM}p_{xy}p_z^1p_z^2p_z^3$ may be used in the region shaded dark grey.

4.3. Concept of groups

Let the laminate have nl layers, or laminae (this also includes the sublaminae). Since all the models given above

have the same representation in terms of the one-dimensional hierarchic basis functions defined over groups of laminae, it is advantageous to define a generic representation of the group structure. The base two-dimensional mesh T_{2D} (with nel_{2D} number of elements) is made first over the projected two-dimensional surface (for example, see Fig. 5(b)). In this study, meshes of triangles are used. Using the base two-dimensional mesh, the three-dimensional mesh T_{3D} of prismatic elements is made over the whole domain, layer by layer. Hence the number of elements in T_{3D} is $nel_{2D} \times nl$. Each two-dimensional element $\tau_{2D} \subseteq T_{2D}$ is assigned the set of all the nl three-dimensional elements $\tau_{3D} \subseteq T_{3D}$, whose projection on the plane is τ_{2D}. This set is denoted as $P_{\tau_{2D}}$. For each element τ_{2D}, the type of model to be used through the thickness is then specified. The model is fixed by the region-by-region allocation described above. Note that two contiguous two-dimensional elements may have the same or different models by this strategy. For the element τ_{2D} we specify the number of groups $ng_{\tau_{2D}}$. For each group $g_{i,\tau_{2D}}, i = 1, 2, \ldots, ng_{\tau_{2D}}$, the three-dimensional elements $\tau_{3D} \subseteq P_{\tau_{2D}}$ contained, are specified. Note that the group will contain one or more three-dimensional elements that are stacked on top of each other. Illustrations of some possible groups is given in Fig. 6, through a frontal view. The figure also demonstrates the possible interfaces between neighboring groups. Note that in this study, case (g) is not considered. Note that the interfaces are the lateral faces and common corner edges of the neighboring three-dimensional elements. Now each group will have its own definition of displacements. We choose the representation of the displacement on the common face or edge to correspond to the "dominant group" of all the groups sharing this edge/face. The dominant group corresponds to the lowest model (e.g. the equivalent model in Fig. 6(b)). Displacements for all neighboring elements will be constrained to follow this representation on the common edge/face.

4.4. Imposition of constraints

In this section, the concept of constrained approximation will be discussed. The ideas are generalization of the concept introduced in [32]. In order to fix ideas let us consider a one-dimensional example. Let us take an interval $(0, L)$ with one element, as shown in Fig. 7(a). Let us also assume that piecewise linear basis functions (i.e. $p = 1$) are defined over this mesh. Let

$$v(z) = \sum_{i=1}^{p+1} a_i M_i(z) \tag{5}$$

be the representation of a function over this domain. Here, $M_i(z)$ are the linear basis functions defined as shown in Fig. 7(a). Let us now subdivide this element into two equal sub-elements, with size $\frac{L}{2}$. Over this new mesh of two elements, let the function $v(z)$, given above, be represented in terms of the piecewise linear basis functions (as shown in Fig. 7(b)) as

$$v(z) = \sum_{i=1}^{2p+1} \bar{a}_i \overline{M}_i(z) \tag{6}$$

where $\overline{M}_i(z)$ are the piecewise linear basis functions defined over the new mesh. Since both Eqs. (5) and (6) represent the same function, the coefficients $\bar{a}_i$ can be expressed in terms of the coefficients a_j. It is obvious that

$$\bar{a}_1 = a_1; \quad \bar{a}_2 = a_2; \quad \bar{a}_3 = \frac{a_1 + a_2}{2} \tag{7}$$

Similarly, the representation of $v(z)$ over any finer mesh can be obtained in terms of the representation over the coarser mesh, with the new fine mesh coefficients $\bar{a}_j$ constrained by the values of the coefficients a_i for the coarser mesh. This can be easily extended to any p order approximation defined over the coarse and fine meshes. As shown below, the transverse representation of the finite element

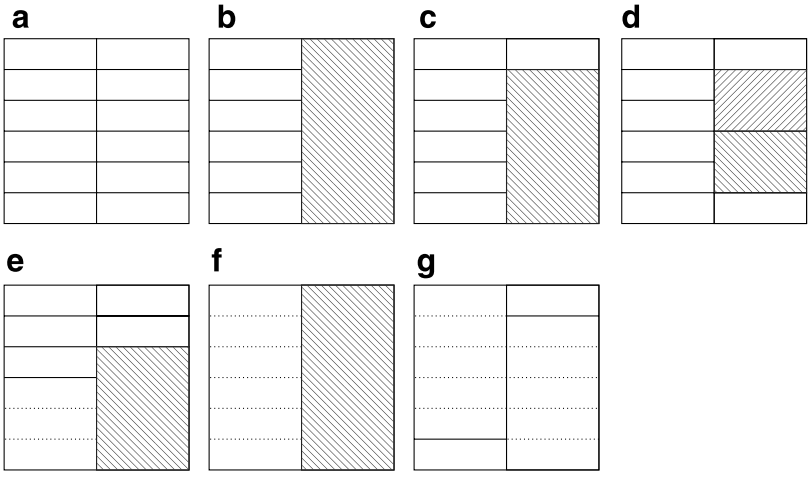

Fig. 6. Illustration of various possible groups of layers in transverse direction. Possible interface conditions between adjacent groups with dominant groups on the interface shown shaded grey.

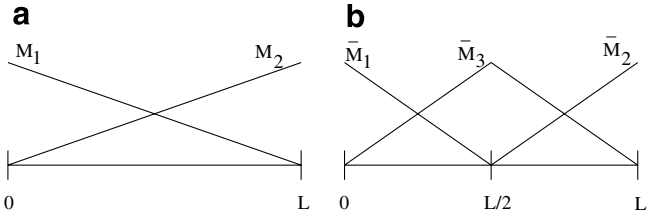

Fig. 7. One-dimensional example of linear constrained approximation.

solution is defined over a group. However, the basic building block in the analysis is the individual three-dimensional element τ_{3D}. Hence, the approach given above will be employed to represent the element degrees of freedom in terms of the group degrees of freedom.

4.4.1. Constraint for a generic group

Let the displacement component $u_1(x,,y,z)$ be given in a group $g_{i,\tau_{2D}}$ (referred as group g in short), by using (1), as

$$u_1^g(x,y,z) = \sum_{j=1}^{N_{1z}} \sum_{i=1}^{N_{2D}} u_{1ij}^g N_i^g(x,y) M_j^g(z) = \sum_{i=1}^{N_{2D}} N_i^g(x,y) \left(\sum_{j=1}^{N_{1z}} u_{1ij}^g M_j^g(z) \right) \tag{8}$$

Here, $N_{2D} = (p_{xy}+1)(p_{xy}+2)/2$; $N_{1z} = (p_z^1+1)$. Note that p_z^1 can be different for each region; N_i^g are the two-dimensional shape functions defined over the projected two-dimensional element τ_{2D}; M_j^g are the one-dimensional hierarchic transverse functions for the group (see Fig. 2). Assuming (as an example) $p_z^1 = 4$, and expanding the transverse approximation, we get

$$u_1^g(x,y,z) = \sum_{i=1}^{N_{2D}} (u_{1i1}^g M_1^g(z) + u_{1i2}^g M_2^g(z) + u_{1i3}^g M_3^g(z) + u_{1i4}^g M_4^g(z) + u_{1i5}^g M_5^g(z)) N_i^g(x,y) \tag{9}$$

Similarly, for an arbitrary element $\tau_{3D} \subseteq g$ (τ in short) the displacement can be written in terms of the element transverse functions (one-dimensional shape functions in the transverse direction) as

$$u_1^\tau(x,y,z) = \sum_{i=1}^{N_{2D}} \left(u_{1i1}^\tau M_1^\tau(z) + u_{1i2}^\tau M_2^\tau(z) + u_{1i3}^\tau M_3^\tau(z) + u_{1i4}^\tau M_4^\tau(z) + u_{1i5}^\tau M_5^\tau(z) \right) N_i^\tau(x,y) \tag{10}$$

Fig. 8 gives the representation of the transverse functions for the element and the group. Since, for any point (x,y,z) in the element τ, $u_1^\tau(x,y,z) = u_1^g(x,y,z)$, the transverse functions $M_i^g(z)$ for the group g can be represented in terms of the transverse functions $M_j^\tau(z)$ for the element as

$$\begin{aligned} M_1^g(z) &= \alpha_1 M_1^\tau(z) + \alpha_2 M_2^\tau(z) \\ M_2^g(z) &= \beta_1 M_1^\tau(z) + \beta_2 M_2^\tau(z) \\ M_3^g(z) &= \gamma_1 M_1^\tau(z) + \gamma_2 M_2^\tau(z) + \gamma_3 M_3^\tau(z) \\ M_4^g(z) &= \delta_1 M_1^\tau(z) + \delta_2 M_2^\tau(z) + \delta_3 M_3^\tau(z) + \delta_4 M_4^\tau(z) \\ M_5^g(z) &= \lambda_1 M_1^\tau(z) + \lambda_2 M_2^\tau(z) + \lambda_3 M_3^\tau(z) + \lambda_4 M_4^\tau(z) + \lambda_5 M_5^\tau(z) \end{aligned} \tag{11}$$

For convenience, the z coordinate in the group is transformed to the master coordinate ξ ($-1 \leqslant \xi \leqslant 1$) using standard linear one-dimensional transformations. The original and the mapped transverse coordinates are shown in Fig. 9. In the mapped coordinates, the extremities of the element are given by ξ_1^τ and ξ_2^τ (as shown in Fig. 9).

For all of the transverse approximation orders the coefficients corresponding to linear part, e.g. α_1, α_2; γ_1, γ_2, etc. are obtained from the values of $M_i^g(z)$ at the nodes. Thus, for $M_1^g(z)$ at ξ_1^τ the first of (11) gives

$$M_1^g(\xi_1^\tau) = \alpha_1 M_1^\tau(\xi_1^\tau) + \alpha_2 M_2^\tau(\xi_1^\tau) = \alpha_1 + 0 \tag{12}$$

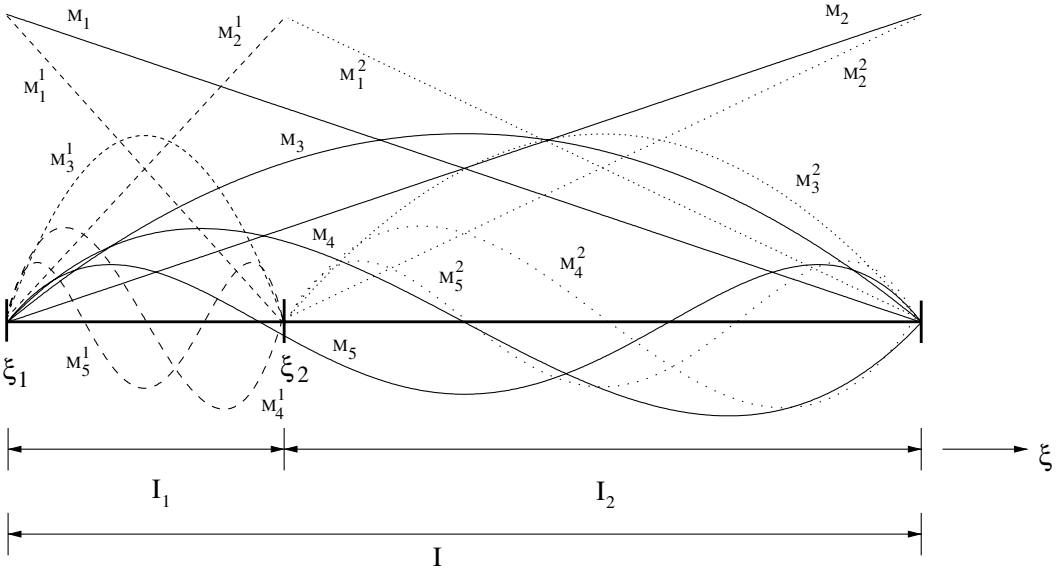

Fig. 8. One-dimensional example of constraint imposition of higher order transverse approximation.

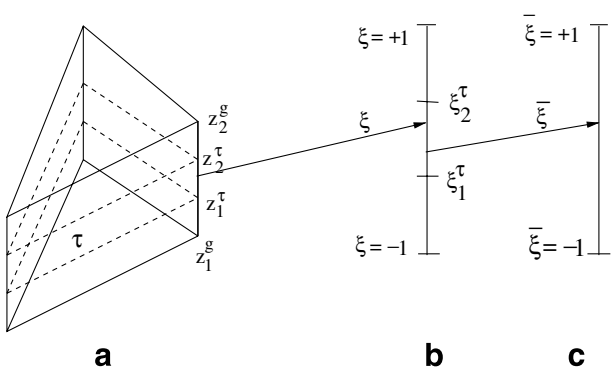

Fig. 9. Example of constraint imposition for element approximation: (a) Typical 3D element τ with extremities of group given by z_1^g, z_2^g with transverse location of element z_1^τ, z_2^τ; (b) the corresponding location of element (ξ_1^τ, ξ_2^τ) with respect to mapped group transverse coordinate ξ; (c) the mapped transverse coordinate system of element given by $\bar{\xi}$.

Thus

$$\alpha_1 = M_1^g(\xi_1^\tau) \quad \text{and similarly} \quad \alpha_2 = M_1^g(\xi_2^\tau) \tag{13}$$

Similarly, other constants are given as

$$\beta_1 = M_2^g(\xi_1^\tau), \quad \beta_2 = M_2^g(\xi_2^\tau), \quad \gamma_1 = M_3^g(\xi_1^\tau), \quad \gamma_2 = M_3^g(\xi_2^\tau)$$
$$\delta_1 = M_4^g(\xi_1^\tau), \quad \delta_2 = M_4^g(\xi_2^\tau), \quad \lambda_1 = M_5^g(\xi_1^\tau), \quad \lambda_2 = M_5^g(\xi_2^\tau)$$

Knowing the constants γ_1 and γ_2 the constant γ_3 is determined from (11), using the following projection:

$$\gamma_3 = \frac{\int_{\xi_1^\tau}^{\xi_2^\tau} \left[M_3^g(\xi) - \left(\gamma_1 M_1^\tau(\xi) + \gamma_2 M_2^\tau(\xi)\right)\right] M_3^\tau(\xi)\mathrm{d}\xi}{\int_{\xi_1^\tau}^{\xi_2^\tau} \left(M_3^\tau(\xi)\right)^2 \mathrm{d}\xi} \tag{14}$$

Similarly, knowing δ_1 and δ_2 the constants δ_3 and δ_4 can be found using (11) from the two equations given by

$$\int_{\xi_1^\tau}^{\xi_2^\tau} [M_3^g(\xi) - (\delta_1 M_1^\tau(\xi) + \delta_2 M_2^\tau(\xi))] M_3^\tau(\xi)\mathrm{d}\xi$$
$$= \delta_3 \int_{\xi_1^\tau}^{\xi_2^\tau} (M_3^\tau(\xi))^2 \mathrm{d}\xi + \delta_4 \int_{\xi_1^\tau}^{\xi_2^\tau} (M_3^\tau(\xi))(M_4^\tau(\xi))\mathrm{d}\xi$$

and

$$\int_{\xi_1^\tau}^{\xi_2^\tau} [M_4^g(\xi) - (\delta_1 M_1^\tau(\xi) + \delta_2 M_2^\tau(\xi))] M_4^\tau(\xi)\mathrm{d}\xi$$
$$= \delta_3 \int_{\xi_1^\tau}^{\xi_2^\tau} (M_3^\tau(\xi))(M_4^\tau(\xi))\mathrm{d}\xi + \delta_4 \int_{\xi_1^\tau}^{\xi_2^\tau} (M_4^\tau(\xi))^2 \mathrm{d}\xi$$

Similarly, three simultaneous equations are solved for λ_3, λ_4 and λ_5. Using (11) in (9) and collecting the coefficients of M_i^τ, we get the representation of u_{lij}^τ in terms of u_{lij}^g.

Note that these coefficients can be obtained symbolically in terms of the extremities ξ_1^τ, ξ_2^τ of the generic element τ. Since this involves only master element coordinates (in the thickness direction), the generic computations can be symbolically done a priori and the explicit expressions can be obtained by putting in the required ξ^τ coordinates. Further, these expressions can be used for any member of any group. Also, the same expressions are valid for the displacement components u_2^g, u_3^g and hence do not have to be recomputed. This procedure is a generalized adaptation of the procedure outlined in [32]. Note that this procedure can be employed to get constraints for any order of approximation in the transverse direction.

4.4.2. Constraint for lateral faces of element τ

Following (9), the constraint has to be applied for all degrees of freedom of the elements τ. As an example, consider the 3D element given in Fig. 10, where $p_{xy} = 3$ and $p_z^i = 2$. Also, consider the displacement component u_k^τ. In the figure, $u_l \equiv u_{kij}$ where $l = (j-1)N_{2D} + i$. The degrees of freedom 10, 20, 30 are internal; degrees of freedom 1, 11, 21, 2, 12, 22, 3, 13, 23 are corner edge degrees of freedom and the rest are degrees of freedom on lateral faces. For the internal degrees of freedom, the transformation given by (11)–(14) will be used. The corner edges and lateral faces of τ are shared with neighboring groups (see Fig. 11). Examples of types of the interfaces are shown in Fig. 6 (dominant groups are shown with grey shade). The displacement on the face is constrained to be that of the dominant group. For the representation of the displacements on the face,

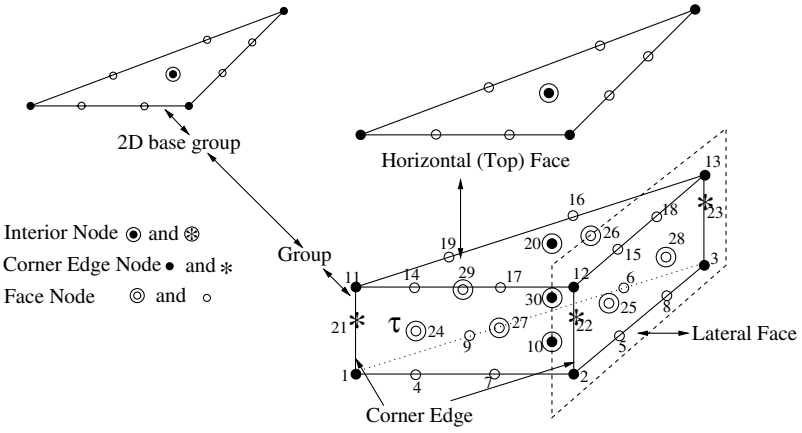

Fig. 10. A generic 3D element with cubic in-plane approximation and quadratic transverse approximation: The interior, edge and face degrees of freedom are shown.

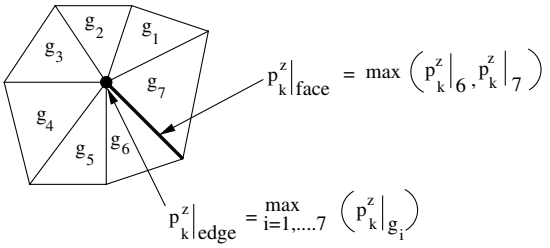

Fig. 11. A generic group cluster with the depiction of the transverse order of approximation for a common edge and a common face. $p_k^z|_{g_i}$ represents the transverse order of approximation for the given group g_i.

p_z^i is chosen to be the maximum of that for the two neighboring groups sharing the face. From Fig. 10, this process will be done for all the face degrees of freedom of the element τ. The constraint matrix for these degrees of freedoms are then obtained by the same procedure as given above. As an example, let all elements τ_{3D} in g_6 (in Fig. 11) have the model EQ3112 while all elements in g_7 have the model LM3332. Then the common face between elements of g_6 and g_7 will follow the displacement representation given by EQ3332 where "EQ" is the dominant group and $p_z^k|_{\max}$ is given by $(3,3,2)$.

4.4.3. Constraint for corner edge of element τ

For the corner edges, the dominant group is determined out of all the groups sharing this edge. The value of p_z^i is again determined as the maximum order of all the groups sharing this edge. For all the degrees of freedom on the corner edge of the element τ, the constraint matrix is obtained using the procedure outlined above.

Using the constrained representation of the interior, lateral face and corner edge degrees of freedom, the constraint matrix $[A^\tau]$ for the element τ can now be formed, such that

$$\{u^\tau\} = [A^\tau]\{u^G\} \tag{15}$$

where $\{u^\tau\}$ are the element degrees of freedom (unconstrained) and $\{u^G\}$ are the corresponding global degrees of freedom defined using the groups (for the solution process, the groups are the elements over which the approximation is globally defined). Note that when element τ is a group by itself, then $[A^\tau] = [I]$.

As an example, the constraint matrix $[A^\tau]$ for the element τ with $p_{xy} = 1$ and $p_z = 2$ for the displacement u is given as

$$\begin{Bmatrix} u_1 \\ u_2 \\ u_3 \\ u_4 \\ u_5 \\ u_6 \\ u_7 \\ u_8 \\ u_9 \end{Bmatrix}^\tau = \begin{bmatrix} \alpha_1 & \beta_1 & \gamma_1 & 0 & 0 & 0 & 0 & 0 & 0 \\ \alpha_1 & \beta_1 & \gamma_1 & 0 & 0 & 0 & 0 & 0 & 0 \\ \alpha_1 & \beta_1 & \gamma_1 & 0 & 0 & 0 & 0 & 0 & 0 \\ 0 & 0 & 0 & \alpha_2 & \beta_2 & \gamma_2 & 0 & 0 & 0 \\ 0 & 0 & 0 & \alpha_2 & \beta_2 & \gamma_2 & 0 & 0 & 0 \\ 0 & 0 & 0 & \alpha_2 & \beta_2 & \gamma_2 & 0 & 0 & 0 \\ 0 & 0 & 0 & 0 & 0 & 0 & 0 & 0 & \gamma_3 \\ 0 & 0 & 0 & 0 & 0 & 0 & 0 & 0 & \gamma_3 \\ 0 & 0 & 0 & 0 & 0 & 0 & 0 & 0 & \gamma_3 \end{bmatrix} \begin{Bmatrix} u_1 \\ u_2 \\ u_3 \\ u_4 \\ u_5 \\ u_6 \\ u_7 \\ u_8 \\ u_9 \end{Bmatrix}^G \tag{16}$$

Remark 2. If the transverse dimension of all the groups for nodal group case and the groups for the vertical faces are same then the dominating group is the current group itself. The approach given is a generalized combination of the representation given in [32,33].

Remark 3. From the implementation certain embedding properties of the models can be seen. For example, EQ3111 is embedded in EQ3222, EQ3333, LM3111, LM3222, ... However, we cannot show that EQ3222 is embedded in LM3111. Hence, a natural hierarchy of models cannot be strictly given. However, note that the EQ3111 is also embedded in IM3111, which in the limit converges to LM3111 (i.e. when the number of groups is increased to the number of layers).

5. Finite element implementation

5.1. Implementation for LM, EQ and IM models

For a given lth lamina the constitutive relationship, in the principal material directions is given as

$$\{\bar{\sigma}_{(l)}\} = [C_{(l)}]\{\bar{\epsilon}_{(l)}\} \tag{17}$$

where $\{\bar{\sigma}_{(l)}\} = \{\sigma_{11}^{(l)} \ \sigma_{22}^{(l)} \ \sigma_{33}^{(l)} \ \sigma_{23}^{(l)} \ \sigma_{13}^{(l)} \ \sigma_{12}^{(l)}\}^{\mathrm{T}}$ are the stress components for the layer, and $\{\bar{\epsilon}_{(l)}\} = \{\epsilon_{11}^{(l)} \ \epsilon_{22}^{(l)} \ \epsilon_{33}^{(l)} \ \epsilon_{23}^{(l)} \ \epsilon_{13}^{(l)} \ \epsilon_{12}^{(l)}\}^{\mathrm{T}}$ are the strain components for the layer. Here, 1, 2 and 3 correspond to the three principal material directions (see Fig. 12(b)). The constitutive relationship in the global xyz-coordinates (for each lamina) can be obtained as

$$\{\sigma_{(l)}\} = [Q_{(l)}]\{\epsilon_{(l)}\} \tag{18}$$

with $\{\sigma_{(l)}\} = \{\sigma_{xx}^{(l)} \ \sigma_{yy}^{(l)} \ \sigma_{zz}^{(l)} \ \sigma_{yz}^{(l)} \ \sigma_{xz}^{(l)} \ \sigma_{xy}^{(l)}\}^{\mathrm{T}}$ and $\{\epsilon_{(l)}\} = \{\epsilon_{xx}^{(l)} \ \epsilon_{yy}^{(l)} \ \epsilon_{zz}^{(l)} \ \epsilon_{yz}^{(l)} \ \epsilon_{xz}^{(l)} \ \epsilon_{xy}^{(l)}\}^{\mathrm{T}}$; $[Q_{(l)}]$ can be obtained from $[C_{(l)}]$ by transformation from the principal material coordinates to global xyz-coordinates. The potential energy, Π, for the structure is given by

$$\Pi = \frac{1}{2}\int_V \{\sigma(u)\}^{\mathrm{T}}\{\epsilon(u)\}\mathrm{d}V - \int_{R^+\cup R^-} T_3 u_3 \,\mathrm{d}s - \int_{\Gamma_{\mathrm{N}}} (T_1 u_1 + T_2 u_2)\mathrm{d}s \tag{19}$$

where V is the volume enclosed by the plate domain; R^+ and R^- are the top and bottom faces of the plate (see Fig. 12(a)); $T_3(x,y)$ is the applied transverse load on these faces; Γ are the lateral faces with $\Gamma = \Gamma_{\mathrm{N}} \cup \Gamma_{\mathrm{D}}$ and $\Gamma_{\mathrm{N}} =$ Neumann boundary, $\Gamma_{\mathrm{D}} =$ Dirichlet boundary; T_1, T_2 are the tractions specified on the lateral faces (in-plane loading).

The solution to the problem, $\mathbf{u}_{\mathrm{ex}}$, is the minimizer of the total potential, Π, and is obtained from the solution of the following weak problem:

Find $\mathbf{u}_{\mathrm{ex}} \in H^0(\mathbf{V})$ such that

$$\mathscr{B}(\mathbf{u}_{\mathrm{ex}}, \mathbf{v}) = \mathscr{F}(\mathbf{v}) \quad \forall \mathbf{v} \in H^0(\mathbf{V}) \tag{20}$$

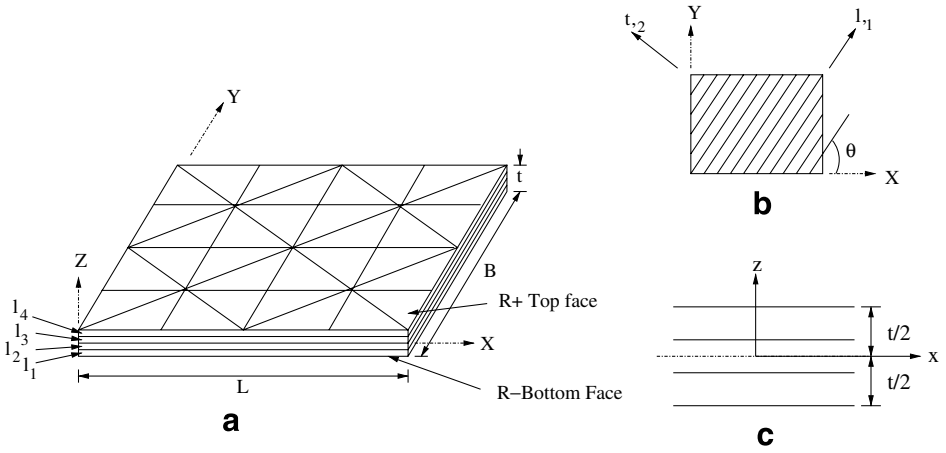

Fig. 12. Global and material directions and laminate configuration.

where $H^0(\mathbf{V}) = \{\mathbf{v} : \mathscr{B}(\mathbf{v},\mathbf{v}) < \infty \text{ and } \mathbf{Mu} = \mathbf{0} \text{ on } \Gamma_D\}$. Note that in this study Dirichlet means the part of lateral boundary where geometric constraints are imposed, while Neumann stands for the parts of the lateral boundary with specified tractions. Further, $\mathbf{M}$ is a generic representation of displacement constraints on the Dirichlet boundary edge. For example, the boundary condition can be clamped; soft simple-support; hard simple-support; etc. (see Table 1 for example). Note that the definition of the Dirichlet boundary conditions can be generalized to include non-homogeneous displacement conditions. The expressions in (20) can be written as

$$\mathscr{B}(\mathbf{u}_{ex},\mathbf{v}) = \sum_l \mathscr{B}_l(\mathbf{u}_{ex},\mathbf{v}) = \sum_l \int_{V_l} \{\sigma_{(l)}(\mathbf{u}_{ex})\}^T \{\epsilon_{(l)}(\mathbf{v})\} dV_l \tag{21}$$

and

$$\mathscr{F}(\mathbf{V}) = \int_{R^+\cup R^+} T_3 v_3 \, ds + \int_{\Gamma_N} (T_1 v_1 + T_2 v_2) ds \tag{22}$$

where V_l is the volume of the lth lamina in the laminate; $\{v\}$ is the test function. Note that in this study T_1, T_2 are taken to be zero on the lateral faces (i.e. the bending problem is considered).

5.2. Implementation for region-by-region model

Eq. (19) can be rewritten as

$$\Pi = \sum_\tau \frac{1}{2}\{u^\tau\}^T [K^\tau]\{u^\tau\} - \{u^\tau\}^T \{F^\tau\} \tag{23}$$

Table 1
Examples of boundary conditions

Boundary	along $x = 0, a$	along $y = 0, b$
Clamped	$u = v = w = 0$	$u = v = w = 0$
Free	$u, v, w \neq 0$	$u, v, w \neq 0$
Hard simple supported	$v = w = 0$	$u = w = 0$
Soft simple supported	$u = w = 0$	$v = w = 0$
Point supported	$w = 0$	$w = 0$

where $\{u^\tau\}$ denotes the displacement vector, $[K^\tau]$ denotes the stiffness matrix and $\{F^\tau\}$ denotes the load vector corresponding to element τ_{3D} (or τ). Using (15), to represent $\{u^\tau\}$, (23) reduces to

$$\Pi = \sum_\tau \frac{1}{2}\{u^G\}^T [A^\tau]^T [K^\tau][A^\tau]\{u^G\} - \{u^G\}^T [A^\tau]^T \{F^\tau\} \tag{24}$$

Minimization of Π gives the matrix problem in terms of $\{u^G\}$, as

$$[K^G]\{u^G\} = \{F^G\}$$

where $[K^G] = \sum_\tau [A^\tau]^T [K^\tau][A^\tau]$ and $\{F^G\} = \sum_\tau [A^\tau]^T \{F^\tau\}$. This gives the constrained element stiffness matrix $[\overline{K}^\tau]$ and load vector $\{\overline{F}^\tau\}$ in terms of the constraint matrix, as

$$[\overline{K}^\tau] = [A^\tau]^T [K^\tau][A^\tau]; \qquad \{\bar{F}^\tau\} = [A^\tau]^T \{F^\tau\} \tag{25}$$

Note that for the given family of models, the implementation is general. The element level stiffness and load computations can be done for each three-dimensional element τ_{3D}. Using the information about the model used locally in the thickness direction, the constraint matrix for the element can be generated. Using this constraint matrix, the constrained element stiffness matrix and load vector can be easily generated. This allows us to use any model in any of the τ_{2D}. Since the method is based on satisfying displacement continuity constraint on the common faces and edges, its extension to other hierarchies of plate models is also possible. Further, note that $[A^\tau]$ can be explicitly computed using the symbolic expressions and hence will not be time consuming. The explicit constant matrix has to be used only at model interfaces. Elsewhere, the model definitions can be directly used.

6. Equilibrium approach of postprocessing

In the present study, the transverse stresses are obtained using both direct approach, i.e. the constitutive equations, and the equilibrium approach.

In the equilibrium approach the three-dimensional equilibrium equations are used to get the transverse stresses from the in-plane stress components. For example

$$\tau_{xz}(x,y,z) = -\int_{z=0}^{z} (\sigma_{xx,x} + \tau_{xy,y})\mathrm{d}z \tag{26}$$

For the right-hand side quantities the constitutive equations are used. Similar procedure for the components τ_{yz} and σ_{zz} is used. For the computation of the postprocessed σ_{zz}, the finite element solution is used to compute $\tau_{xz,x}$ and $\tau_{yz,y}$ (for use in the right-hand side of (26)).

7. Numerical results

The major goal of this paper is to present an approach through which the local three-dimensional state of stress can be obtained in a laminated plate structure, in a designated region of interest, with optimal computational effort. Hence, the local accuracy of the EQ, IM and LM families of plate models will be analyzed first. This will be done by comparing the pointwise stresses with those obtained by the theory of elasticity solution where applicable. This will be followed by a study of the efficacy of region-by-region implementation, for various problems.

The list of models used in the following examples are:

(1) LM3332, EQ3332, IM3332: layerwise, equivalent single layer and intermediate models used in [0/90/0/90/0/90/0/90/0] laminate bending problem.
(2) RR-I, RR-II, RR-III: Region-by-region models used for cylindrical bending of [165/−165] and [150/−150/150] laminates.
(3) RR2332: Region-by-region model for first-ply failure problem.
(4) RR-U, RR-G: Region-by-region models used for domain with multi-material region problem.

7.1. Effect of model on accuracy of pointwise data for EQ, IM and LM models

In this section, the EQ, IM and LM models are compared for the transverse deflection and state of stress.

7.1.1. Comparison of transverse deflection

These models are compared with the exact three-dimensional elasticity solution for seven layer [0/90/0/90/0/90/0] cross-ply, square laminate. Total thickness of 0° layers is equal to total thickness of 90° laminae and laminae of same orientation are of equal thickness. The material properties are as given in Table 2. The plate has dimension $a = b = St$ along x-axis and y-axis, respectively. Here, $S = \frac{a}{t}$ is aspect ratio with $t = 6$ mm. The plate is subjected to transverse sinusoidal loading of the form

$$T_3(x,y) = q_0(x,y)\sin\left(\frac{\pi x}{a}\right)\sin\left(\frac{\pi y}{b}\right)$$

Table 2
Material properties for graphite/epoxy [35,36]

Property	E_{11}	E_{22}	G_{12}	G_{23}	$v_{12} = v_{23}$
Values	25×10^6 psi	10^6 psi	0.5×10^6 psi	0.2×10^6 psi	0.25

All edges of the laminate are soft simple-supported. The transverse deflection ($w = u_3$) is nondimensionalised as $\bar{w} = \frac{\pi^4 Q w(\frac{a}{2},\frac{b}{2},0)}{12 q_0 S^4 t}$, where

$$Q = 4G_{12} + [E_{11} + E_{22}(1 + 2v_{23})]/(1 - v_{12}v_{21})$$

The nondimensional thickness is defined as $\bar{z} = \frac{z}{t}$. The values of $\bar{w}$ are tabulated in Table 3. The models used are LM3332, IM3332 and EQ3332. The number in parenthesis are the percentage error in the computed transverse displacements. Note that for the intermediate model, the bottom four layers of the laminate are lumped together to form an equivalent layer whereas the top three layers are individual layers.

From the table we observe that

1. The LM3332 model predicts the transverse deflection accurately for all the aspect ratios. The error in the values ranges from 0% to 0.008%.
2. The IM3332 and EQ3332 models are far from the exact one for the aspect ratios up to $S = 10$, i.e. for thick plates. The error for these aspect ratios ranges from 3.6% to 12%.
3. For the IM3332 and EQ3332 models with aspect ratios $S > 10$ the displacement is close to exact. The error is 0–2.5%. The IM3332 model is more accurate, as compared to the EQ3332 model.

Remark 4. Explicit discretization error control is not used here. However, sufficiently refined meshes are used a priori to ensure that discretization error is small. The same mesh is used for all the models.

7.1.2. Comparison of state of stress

Here we take the nine layered cross-ply laminate [0/90/0/90/0/90/0/90/0] with the total thickness of 0° layers as that of the 90° layers. The plate has dimensions $a = b = St$ with $t = 10$ mm. All the edges of the plate are soft simple-supported. Note that for IM model the bottom

Table 3
Comparison of transverse displacement ($\bar{w}$) for cross-ply seven layer square laminate under sinusoidal loading

S	Exact [35]	LM3332	IM3332	EQ3332
2	12.342	12.341 (0.008)	11.866 (3.86)	13.790 (−11.73)
4	4.153	4.153 (0.00)	3.846 (7.39)	3.712 (10.62)
10	1.529	1.529 (0.00)	1.473 (3.66)	1.417 (7.32)
20	1.133	1.133 (0.00)	1.119 (1.25)	1.104 (2.55)
50	1.021	1.021 (0.00)	1.019 (0.19)	1.017 (0.39)
100	1.005	1.005 (0.00)	1.005 (0.00)	1.004 (0.09)

six laminae are lumped in single equivalent layer while the remaining three laminae are left as such. The stresses are normalised as

$$(\bar{\sigma}_{xx}, \bar{\sigma}_{yy}, \bar{\tau}_{xy}) = \frac{1}{q_0 S}(\sigma_{xx}(x,y,\bar{z}), \sigma_{yy}(x,y,\bar{z}), \tau_{xy}(x,y,\bar{z}))$$

$$(\bar{\sigma}_{zz}, \bar{\tau}_{xz}, \bar{\tau}_{yz}) = \frac{1}{q_0 S^2}(\sigma_{zz}(x,y,\bar{z}), \tau_{xz}(x,y,\bar{z}), \tau_{yz}(x,y,\bar{z}))$$

The through thickness variation of the normalised in-plane stress $\bar{\sigma}_{xx}$ is plotted at $\left(\frac{a}{2}, \frac{a}{2}, \bar{z}\right)$ for various families of plate models. Similarly, the through thickness variation of the transverse stress $\bar{\tau}_{xz}$ is plotted at $\left(0, \frac{b}{2}, \bar{z}\right)$. All the results are given for $S = 2$ (thick plate) and $S = 10$ (moderately thick plate). For, the transverse stresses, both the direct values obtained from constitutive relationship and those obtained by the equilibrium based postprocessing are plotted in Fig. 13. The models used here are LM3332,

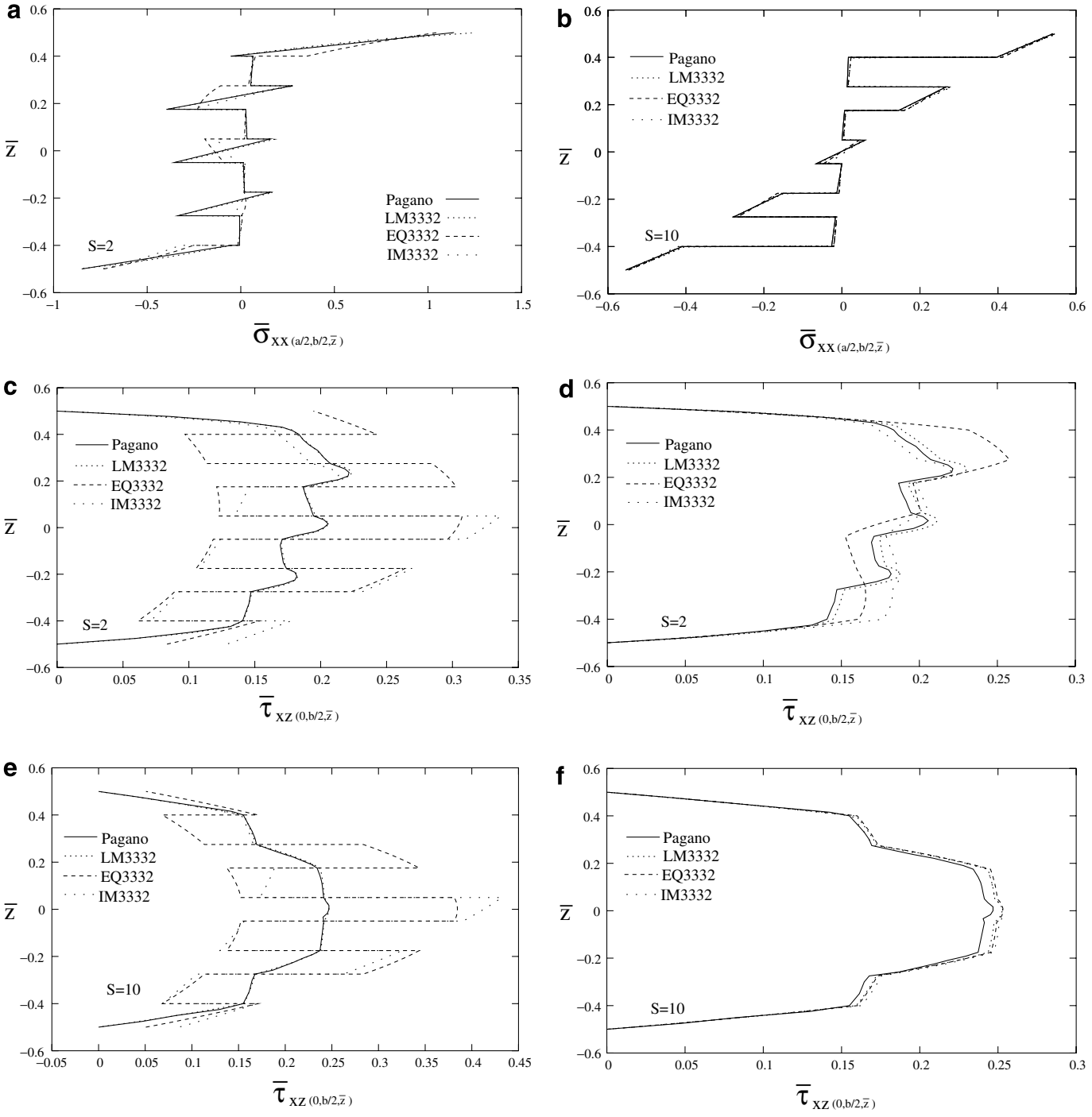

Fig. 13. Comparison of in-plane and transverse shear for 9-layered cross-ply, square laminate; all edges soft simple-supported. (a) Direct stresses ($S = 2$), (b) direct stresses ($S = 10$), (c) direct stresses ($S = 2$), (d) equilibrium based postprocessed stresses ($S = 2$), (e) direct stresses ($S = 10$) and (f) equilibrium based postprocessed stresses ($S = 10$).

EQ3332 and IM3332. The stresses obtained by the various models is compared with the exact three-dimensional values from [35]. The pointwise values of stress components $\bar{\sigma}_{xx}$ and $\bar{\tau}_{xz}$ directly obtained from these models are also given in Tables 4 and 5.

From the figure we note that:

1. The LM3332 model is very accurate for all values of S (the graph overlaps the exact one), for both in-plane and out of plate stress components.
2. The EQ3332 model can have significant errors in $\bar{\sigma}_{xx}$ for thick laminates. However, as S increases the $\bar{\sigma}_{xx}$ becomes more accurate. For $S = 10$, the error in pointwise $\bar{\sigma}_{xx}$ is very small.
3. The directly computed $\bar{\tau}_{xz}$ obtained using EQ3332 model is different from the exact one both qualitatively and quantitatively.
4. The directly computed $\bar{\sigma}_{xx}$, $\bar{\tau}_{xz}$ for IM3332 model is close to the EQ3332 for bottom 6 laminae (which are lumped together for analysis), while in the top three laminae the values of the stresses are close to the exact one. In this case even $\bar{\tau}_{xz}$, obtained directly, is reasonably accurate in the top three-layers.
5. For the EQ3332 and IM3332 models, equilibrium based postprocessing, is effective in giving reasonably accurate representation of the transverse stress components.
6. For $S = 2$, the EQ3332 model is inaccurate, as compared to the IM3332 and LM3332 models.

Table 4
Pointwise values of stress component $\bar{\sigma}_{xx}\left(\frac{a}{2}, \frac{b}{2}, \bar{z}\right)$ for [0/90/0/90/0/90/0/90/0], $S = 10$, laminate under sinusoidal loading

$\bar{z}$	Pagano [35]	LM	EQ	IM
0.500	0.541	0.540	0.547	0.540
0.400	0.396	0.399	0.411	0.397
0.400	0.016	0.016	0.023	0.022
0.275	0.013	0.013	0.015	0.016
0.275	0.267	0.265	0.265	0.281
0.175	0.145	0.146	0.163	0.158
0.175	0.006	0.006	0.009	0.009
0.050	0.000	0.000	0.003	0.003
0.050	0.059	0.058	0.044	0.053
−0.050	−0.066	−0.062	−0.047	−0.037
−0.050	0.000	0.000	−0.001	0.000
−0.175	−0.013	−0.012	−0.007	−0.007
−0.175	−0.152	−0.150	−0.165	−0.160
−0.275	−0.277	−0.277	−0.267	−0.268
−0.275	−0.016	−0.016	−0.013	−0.013
−0.400	−0.026	−0.025	−0.021	−0.021
−0.400	−0.409	−0.404	−0.412	−0.419
−0.500	−0.554	−0.549	−0.547	−0.554

Table 5
Pointwise values of stress component $\bar{\tau}_{xz}\left(0, \frac{b}{2}, \bar{z}\right)$ for [0/90/0/90/0/90/0/90/0], $S = 10$, laminate under sinusoidal loading

$\bar{z}$	Pagano [35]	LM3332	EQ3332	IM3332
−0.500	0.000	0.000	0.051	0.086
−0.400	0.155	0.155	0.171	0.170
−0.400	0.155	0.155	0.068	0.068
−0.275	0.167	0.168	0.113	0.104
−0.275	0.167	0.168	0.284	0.262
−0.175	0.237	0.237	0.343	0.325
−0.175	0.237	0.237	0.137	0.130
−0.050	0.241	0.241	0.152	0.156
−0.050	0.241	0.241	0.381	0.390
0.050	0.241	0.241	0.381	0.432
0.050	0.241	0.241	0.152	0.173
0.175	0.234	0.236	0.137	0.188
0.175	0.234	0.236	0.343	0.237
0.275	0.169	0.168	0.284	0.165
0.275	0.169	0.168	0.113	0.165
0.400	0.155	0.154	0.068	0.153
0.400	0.155	0.154	0.171	0.153
0.500	0.000	0.000	0.051	0.000

From the results of this section we observe that the LM model is very accurate with respect to the pointwise data. However, the cost of computation increases significantly when this model is used. Generally, we are interested in the state of stress in a particular region, in only a few critical laminae. Note that the IM model can be effectively used to zoom onto desired laminae. For example, if the top lamina is of interest, then the top two or three laminae can be taken as separate layers, while remaining laminae can be lumped into an equivalent layer. This leads to significant saving in computational cost, without much degradation in accuracy. Also note that the higher (more expensive) models need to be used only in a reasonable neighborhood of the region of interest. Elsewhere a lower model, e.g. EQ model, can be used, to lead to further saving in computational cost. Below, we

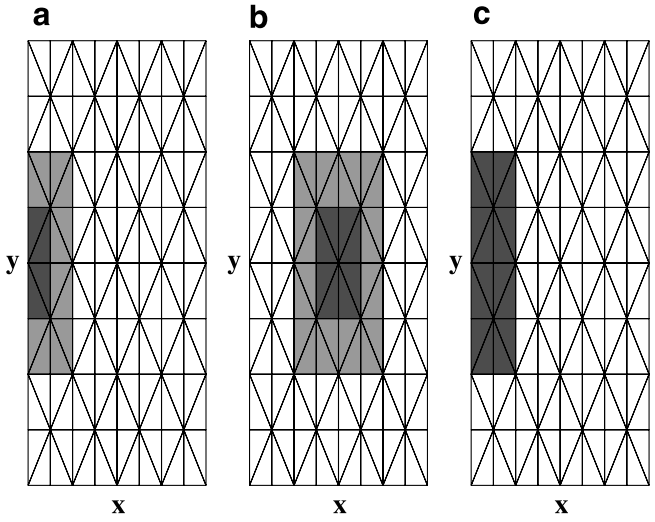

Fig. 14. Region-by-region schemes for transverse shear and in-plane stress for [165/−165] and [150/−150/150] laminate. (a) RR-I: with LM3332 in the dark shaded region, LM3112 in the grey shaded region and EQ3112 in the rest, (b) RR-II: with LM3332 in the dark shaded region, LM3112 in the grey shaded region and EQ3112 in the rest and (c) RR-III: with LM3332 in the dark shaded region and EQ3112 in the rest.

demonstrate through numerical examples the efficacy of such an implementation.

7.2. Region-by-region modeling

Here we consider various types of problems to study the accuracy of the region-by-region modeling approach. This modeling approach is compared with EQ, LM and IM models.

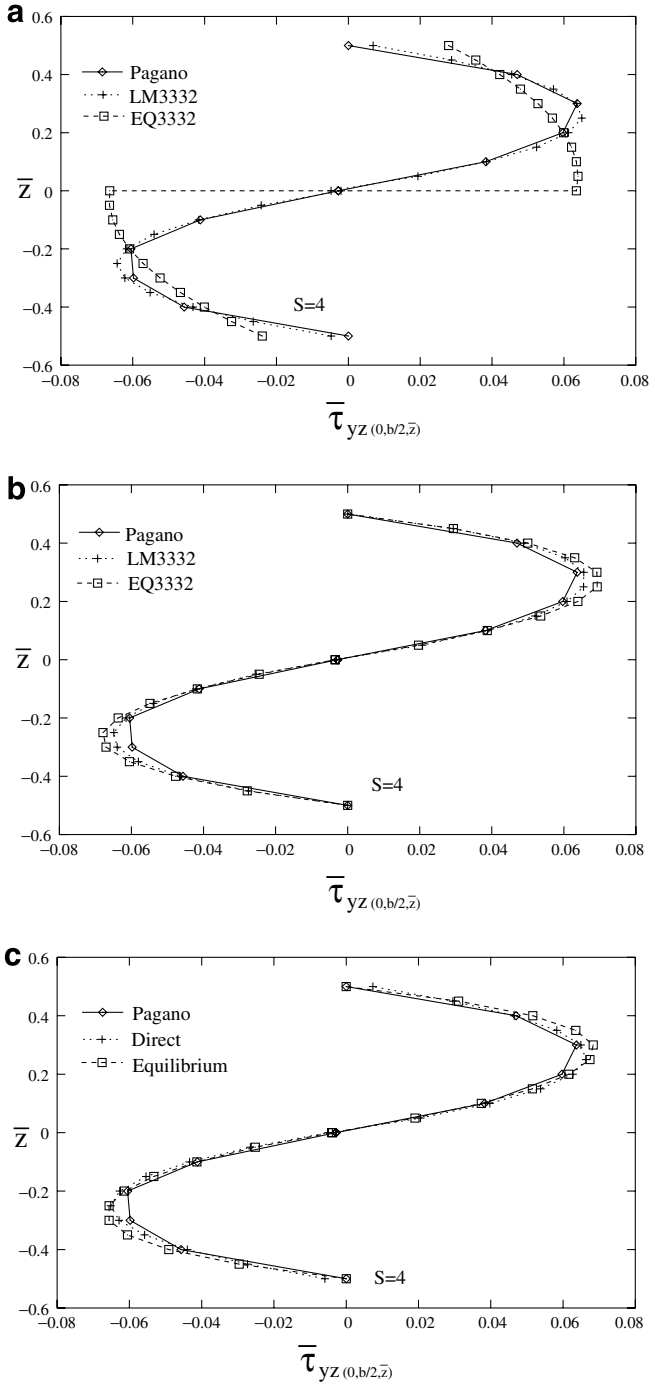

Fig. 15. Comparison of transverse shear stress for [165/−165] laminate under cylindrical bending. (a) Direct stresses, (b) equilibrium based postprocessed stresses and (c) region-by-region scheme I (RR-I).

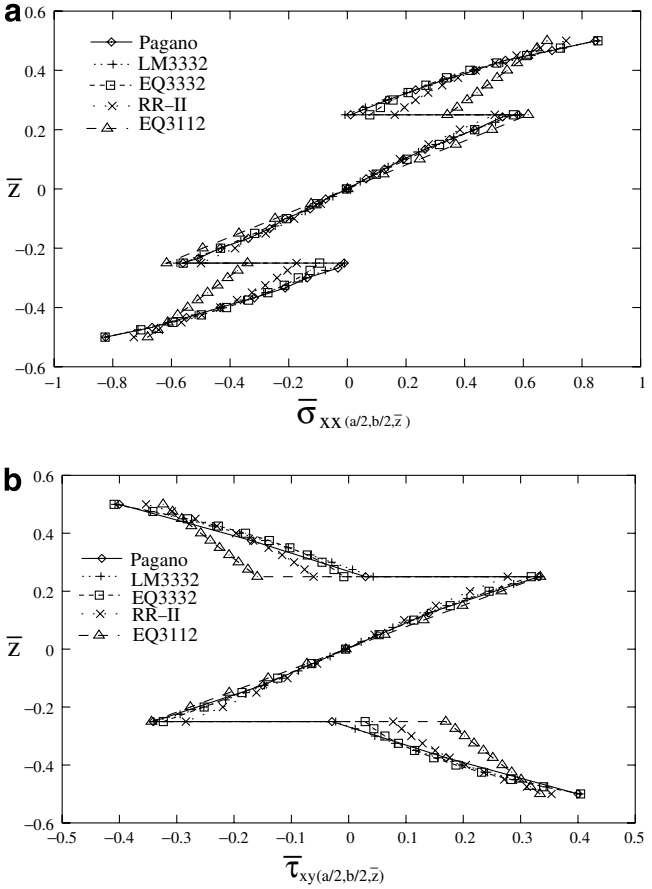

Fig. 16. Comparison of in-plane stresses for [150/−150/150] laminate under cylindrical bending. (a) In-plane normal stress and (b) in-plane shear stress.

7.2.1. Cylindrical bending problems

Here, various stress components for symmetric and anti-symmetric laminates, under cylindrical bending, are compared with the exact values given in [36]. The cylindrical bending load is of the form $T_3(x,y) = q_0 \sin\left(\frac{\pi x}{a}\right)$. The LM3332 and EQ3332 models are used for computing the stresses.

Case 1 (*Point at Boundary*): In this case [165/−165] laminate is considered. All the laminae are of equal thickness. Here, we have taken $t = 2nl$ ($t = 2$ mm here) and $a = St$. Further, in the y-direction the plate is taken to be sufficiently long with $b = 20a$. At $x = 0$, a the edge is point supported while at $y = 0$, b the edge is free. The normalised stress $\bar{\tau}_{yz}$ is plotted at $(0, \frac{b}{2}, \bar{z})$. The region-by-region scheme I (RR-I) for this case is shown in Fig. 14(a). In the darker region LM3332 model is used. In the region shown by grey shading LM3112 model is used followed by the EQ3112 model in the remaining region. The stress components for $S = 4$ are shown in Fig. 15.

Case 2 (*Interior and Boundary Point*): Here, [150/−150/150] laminate is considered such that the thickness of each layer is $[1, 2, 1]$ and $t = 4$ mm. The truncated mesh (in the y-direction) used for this example is shown in Fig. 14. The normalised in-plane stresses $\bar{\sigma}_{xx}$ and $\bar{\tau}_{xy}$ are plotted at $(\frac{a}{2}, \frac{b}{2}, \bar{z})$ while the transverse shear stresses are plotted at

$(0,\frac{b}{2},\bar{z})$. Since the transverse stresses are shown for a point on the boundary, the RR-I scheme is used for these results. The in-plane stresses are given for an interior point, hence, the RR-II scheme shown in Fig. 14(b) is used. Here the darker region has LM3332, grey region has LM3112 and remaining region has EQ3112. The transverse shear stresses are also obtained by another scheme (RR-III) shown in Fig. 14(c) where the darker region has EQ3332 and remaining region has EQ3112 model. Note that the results are also obtained by using EQ3332, EQ3112 and LM3332 models in the full domain for comparison with the, RR-II and RR-III schemes. The in-plane stresses and transverse shear stresses for $S = 4$ are shown in Figs. 16 and 17, respectively. The stresses obtained in case 1 and case 2 are compared with the exact three-dimensional values from [36]. The pointwise values of stress component $\bar{\tau}_{xz}$ at $(0,\frac{b}{2},\bar{z})$ directly obtained from these models are also given in Table 6.

From the results it is observed that:

1. All the stress components obtained directly by the LM3332 model are close to the exact values.
2. The direct transverse stresses obtained by the EQ3332 and RR-III models are almost the same but are qualitatively and quantitatively different from the exact one. Using the RR-I model gives better direct values of transverse stresses.
3. When the equilibrium based postprocessing is employed the EQ3332 and RR-III models give very good values of transverse stresses while RR-I model leads to slightly inferior accuracy of the transverse stresses. This is because the EQ3332 model (and RR-III model) lead to more accurate in-plane stresses in the neighborhood of point of interest while RR-I model may lead to less accurate values of in-plane stresses in this neighborhood. The equilibrium based postprocessing approach uses the derivatives of in-plane stresses to obtain the transverse stresses.

The quality of the solution can be further improved by enriching the local model further. For example, one can use the LM3332 model in a one layer neighborhood of the region of interest.

In Table 7, the number of unknowns for all the models used in these cases are compared. From this table it is observed that:

1. The LM3332 approach is very intensive computationally.

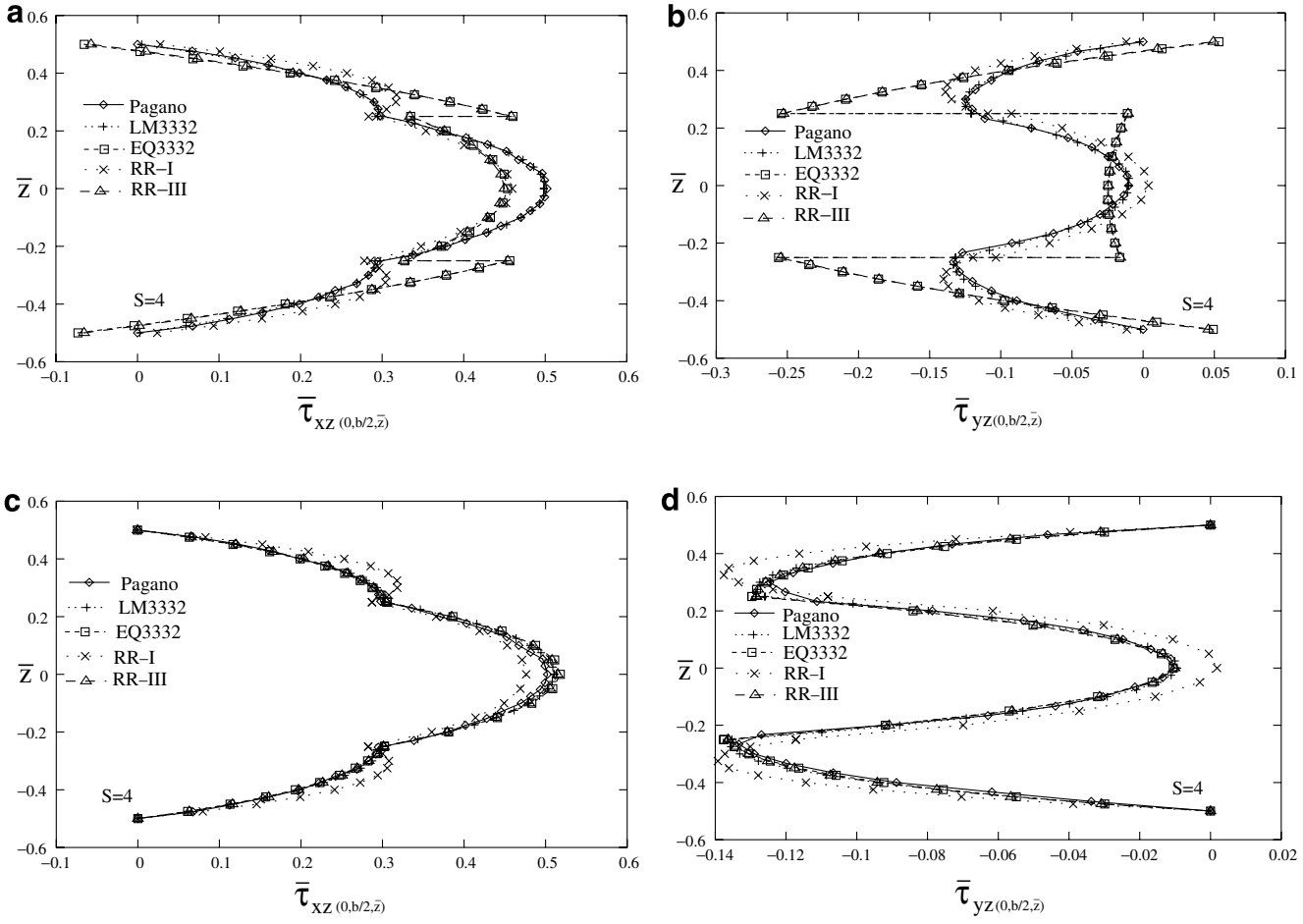

Fig. 17. Comparison of transverse shear stresses for [150/−150/150] laminate cylindrical bending for point at boundary $(0,\frac{b}{2},\bar{z})$. (a) Direct stress, (b) direct stress, (c) equilibrium based postprocessed stress and (d) equilibrium based postprocessed stress.

Table 6
Pointwise values of stress component $\bar{\tau}_{xz}\left(0,\frac{b}{2},\bar{z}\right)$ for [150/−150/150], $S=4$, laminate under cylindrical bending loading

$\bar{z}$	Pagano [36]	LM3332	EQ3332	RR-I	RR-III
0.500	0.000	0.005	−0.065	0.027	−0.056
0.400	0.198	0.200	0.187	0.256	0.190
0.300	0.290	0.289	0.383	0.316	0.383
0.200	0.371	0.375	0.378	0.293	0.376
0.100	0.467	0.473	0.435	0.434	0.432
0.000	0.502	0.498	0.453	0.452	0.449
−0.100	0.470	0.470	0.433	0.431	0.429
−0.200	0.379	0.273	0.372	0.347	0.370
−0.300	0.283	0.283	0.378	0.305	0.377
−0.400	0.198	0.192	0.181	0.242	0.183
−0.500	0.000	0.003	−0.073	0.024	−0.001

Table 7
Number of unknowns for given choice of model and laminate

Laminate	Model	Stress component	Unknowns
[165/−165]	Throughout LM3332	$\bar{\sigma}_{xx},\bar{\tau}_{xy},\bar{\tau}_{xz},\bar{\tau}_{yz}$	11,875
[150/−150/150]		$\bar{\sigma}_{xx},\bar{\tau}_{xy},\bar{\tau}_{xz},\bar{\tau}_{yz}$	16,875
[165/−165]	Throughout EQ3332	$\bar{\sigma}_{xx},\bar{\tau}_{xy},\bar{\tau}_{xz},\bar{\tau}_{yz}$	6875
[150/−150/150]		$\bar{\sigma}_{xx},\bar{\tau}_{xy},\bar{\tau}_{xz},\bar{\tau}_{yz}$	6875
[165/−165]	Region-by-region (scheme I)	$\bar{\tau}_{xz},\bar{\tau}_{yz}$	4863
[150/−150/150]	Region-by-region (scheme II)	$\bar{\sigma}_{xx},\bar{\tau}_{xy}$	5147
[150/−150/150]	Region-by-region (scheme I)	$\bar{\tau}_{xz},\bar{\tau}_{yz}$	5239
[150/−150/150]	Region-by-region (scheme III)	$\bar{\tau}_{xz},\bar{\tau}_{yz}$	4715

2. The RR-I, RR-II and RR-III schemes lead to tremendous saving in computational cost, as compared to LM3332 (or EQ3332 model for RR-III), and also give local accuracies comparable to the LM3332 model (or EQ3332 model for RR-III).

7.2.2. First-ply failure load prediction

The first-ply failure load is obtained by using Tsai–Wu criterion is given by (see [37,38] for more details)

$$FI_{\mathrm{TW}} = F_i\sigma_i + F_{ij}\sigma_i\sigma_j \geqslant 1 \tag{27}$$

where F_i and F_{ij} are the strength tensor terms and σ_i are the stress components. As an example the [−45/45/−45/45] is taken. The plate is clamped on all edges. The top face of the plate is subjected to uniform transverse load $T_3(x,y)=q_0$. The plate dimensions are $a=228.9$ mm (9 in.), $b=127$ mm (5 in.). The material properties and lamina thickness used in these computations are given in Table 8. The first-ply failure load is nondimensionalised as

$$\mathrm{FLD} = \frac{q_0}{E_{22}}S^4$$

Table 8
Material properties for T300/5208 Graphite/Epoxy (Pre-preg) [38]

Property	Value	Property	Value
E_{11}	132.5 GPa	X_{T}	1515 MPa
$E_{22}=E_{33}$	10.8 GPa	X_{C}	1697 MPa
$G_{12}=G_{13}$	5.7 GPa	$Y_{\mathrm{T}}=Z_{\mathrm{T}}=Y_{\mathrm{C}}=Z_{\mathrm{C}}$	43.8 MPa
G_{23}	3.4 GPa	R	67.6 MPa
$v_{12}=v_{13}$	0.24	$S=T$	86.9 MPa
v_{23}	0.49	Ply thickness, t_i	0.127 mm

The results obtained from the present analysis are compared with those reported in [38]. The loads are computed using LM2332, EQ2332 and RR2332. For the region-by-region model (RR2332 as shown in Fig. 18) the failure load is first computed by equivalent single layer model. The elements with failure index above 0.8 are found. These will be the critical region of interest or "hot-spots". In a neighborhood of this region, it is desired to enrich the model to get the three-dimensional state of stress more accurately. In the implementation in one element neighborhood of these elements (shaded dark grey in Fig. 18) the LM2332 model is used, while in the remaining region the EQ2332 model is used. The first-ply failure load is given in Table 9.

In the present study, the transverse stress components obtained from the equilibrium based postprocessing approach, have been used in computing the failure load.

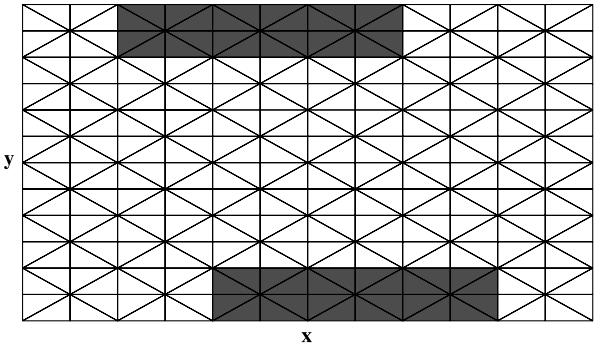

Fig. 18. [−45/45/−45/45] laminate with clamped boundaries: Regions with $FI_{\mathrm{TW}} \geqslant 0.8$ shown shaded grey.

Table 9
First-ply failure loads; all edges clamped, [−45/45/−45/45] laminate under uniform transverse loading, $p_{xy}=2$

Model	FLD	Coordinates		Layer	Location	Unknowns	Max. σ
		x	y				
Reddy [38]	39354.8	≈115.00	≈125.00	1	Bottom	–	–
EQ2332	32382.6	121.38	126.43	1	Bottom	6875	σ_{22}
RR2332	32386.1	107.51	0.56	1	Bottom	8987	σ_{22}
LM2332	32549.2	107.51	0.56	1	Bottom	21,875	σ_{22}

We observe that:

1. The first-ply failure loads obtained by RR2332 and LM2332 models are close.
2. The locations predicted by the RR2332 and LM2332 models are close.
3. The number of unknowns for LM2332 model are significantly higher as compared to the RR2332 model.

The locations and values obtained by LM2332 and RR2332 are not the same as [38] because the mesh and the model used here is more refined. Note that the solution of [38] is "stiffer" leading to higher predicted failure loads. This could be dangerous from a design point of view. Using adaptivity (with a fixed model) for discretization error control would have led to a further reduction in the predicted failure load (see [11] for details).

7.3. Domain with multi-material region

Let us take the rectangular domain of Fig. 19(c). The dimensions of the plate are $a = 100$ mm, $b = 10$ mm and $t = 0.254$ mm. The plate is clamped along all the edges and is subjected to a uniform transverse load of intensity $q_0 = 1\ \mathrm{N/mm^2}$. The plate has two lamina with [0/90] in the regions $0 \leqslant x \leqslant \frac{a}{2}$, $0 \leqslant y \leqslant b$. The material properties for each lamina are as given in Table 8. In the region $\frac{a}{2} \leqslant x \leqslant a$, $0 \leqslant y \leqslant \frac{b}{2}$, the plate has a bottom layer of epoxy (with $E_{11} = E_{22} = E_{33} = 4600$ MPa, $v_{12} = v_{13} = v_{23} = 0.36$) for $-\frac{t}{2} \leqslant z \leqslant 0$. For $z \geqslant 0$, lamina with 90° orientation with material properties given in Table 8 is present (see Fig. 19(a)). The plate essentially mimics a L-shaped domain in two-dimensions. For this domain the exact solution will have an edge singularity along the line given by $x = \frac{a}{2}$, $z = 0$. To solve this problem we will use LM3333, EQ3333 models and the region-by-region schemes given by:

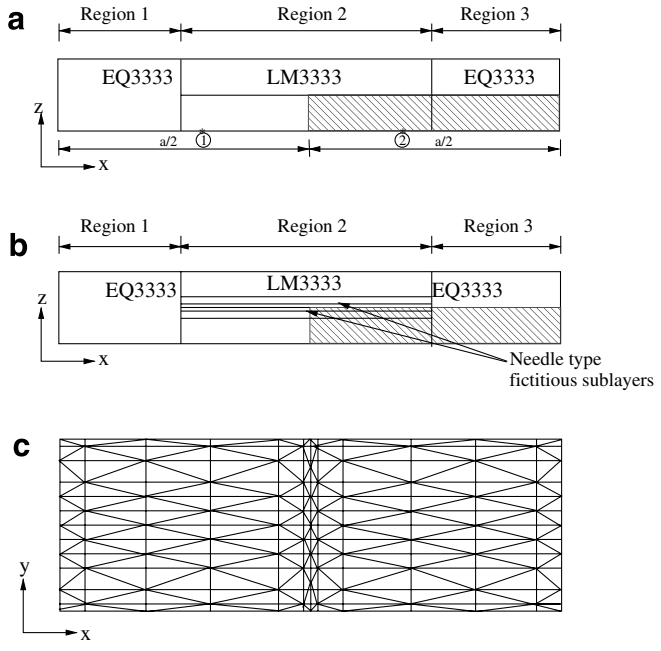

Fig. 19. Multimaterial beam problem: mesh and model. (a) RR-U model with point of interest, (b) RR-G model and (c) the two-dimensional mesh.

1. RR-U (Fig. 19(a)): EQ3333 in region 1, LM3333 model in region 2 and 3.
2. RR-G (Fig. 19(b)): EQ3333 in region 1, LM3333 model in region 2 and 3, with geometrically graded sublaminae (with factor $q = 0.15$) near $z = 0$.

Note that in the RR strategies the 3D model is used in the vicinity of the singular edge only. Elsewhere, lower models are used.

Remark 5. The two-dimensional mesh is as shown in Fig. 19(c), with geometrically graded elements (with grading factor $q = 0.15$) in the vicinity of the line $x = \frac{a}{2}$. The energy norm of the discretization error, e_{D}, for this mesh was 2.84% (when the EQ3333 model is used everywhere). For this mesh, we can assume that the major contributor to the error is modeling error e_{M}, i.e. the total error $\mathbf{e} = \mathbf{u}_{3\mathrm{D}} - \mathbf{u}_{\mathrm{M}} + \mathbf{u}_{\mathrm{M}} - \mathbf{u}_{\mathrm{FE}} = \mathbf{e}_{\mathrm{M}} + \mathbf{e}_{\mathrm{D}} \approx \mathbf{e}_{\mathrm{M}}$. Here the exact three-dimensional solution to the problem is denoted by $\mathbf{u}_{3\mathrm{D}}$; the exact solution to the chosen model is given by $\mathbf{u}_M$; the finite element solution for the chosen model (for the given mesh and in-plane approximation) is given by $\mathbf{u}_{\mathrm{FE}}$. Note further that the RR-G scheme leads to elements with high aspect ration in the vicinity of the singular edge.

7.3.1. Displacement analysis

The displacement components, along a cutting line given by $y = \frac{b}{2}$, $z = \frac{t}{2}$, is plotted in Fig. 20. From the figure we observe that:

1. The LM3333 and RR-U strategies give almost identical displacement profiles.
2. The displacement due to the EQ3333 model is far from LM3333 and RR-U models at the boundary and in the region of material dissimilarity.
3. The displacements have a sharp change at $x = \frac{a}{2}$. This is because the effective flexural rigidity reduces significantly beyond $x = \frac{a}{2}$.

The results clearly bring out the effect of pollution in the modeling error as explained below.

For the EQ3333 model the modeling error is significant in the vicinity of the singular edge (when compared to the LM3333 or RR-U models). This affects the local quality of the displacements and stresses at the regions far from the corner. For example, let us take the average displacement $v_{i,\mathrm{avg}}$, in a small region $\bar{v}$ near the boundary, given by $v_{i,\mathrm{avg}} = \frac{1}{\bar{v}} \int_{\bar{v}} v_i \, \mathrm{d}v$. Let $v_{i,\mathrm{avg}}^{\mathrm{LM}}$ be the quantity when the LM3333 model is used everywhere, with the refined mesh shown in Fig. 19(c). Similarly, let $v_{i,\mathrm{avg}}^{\mathrm{EQ}}$ be the quantity obtained using the EQ3333 model everywhere with the

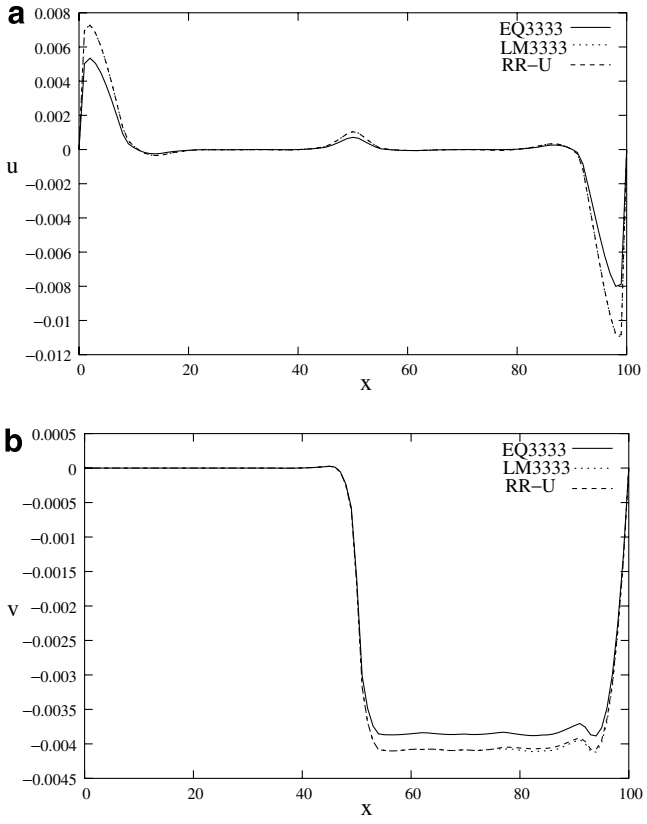

Fig. 20. Displacements variation on the top face of the beam, along the line $y = \frac{h}{2}$. (a) u displacement, (b) v displacement and (c) w displacement.

same mesh. Following [11], we can solve for the dual function G_i^{LM} (using the same mesh and LM3333 models) as

$$\mathscr{B}\left(G_i^{\mathrm{LM}}, \mathbf{v}^{\mathrm{LM}}\right) = \frac{1}{\bar{v}} \int_{\bar{v}} v_{i,\mathrm{avg}}^{\mathrm{LM}} \, \mathrm{d}v \tag{28}$$

where $\mathbf{v}^{\mathrm{LM}}$ is represented in terms of the LM3333 model; G_i^{LM} satisfies homogeneous Dirichlet boundary conditions on the clamped edges. Since the displacement u_i^{EQ} (corresponding to EQ3333 model) can be represented in terms of the basis functions corresponding to LM3333 model, $\mathbf{v}^{\mathrm{LM}} = \mathbf{u}^{\mathrm{LM}} - \mathbf{u}^{\mathrm{EQ}}$ can be chosen. Hence

$$\begin{aligned}\mathscr{B}\left(G_i^{\mathrm{LM}}, \mathbf{u}^{\mathrm{LM}} - \mathbf{u}^{\mathrm{EQ}}\right) &= \left(u_{i,\mathrm{avg}}^{\mathrm{LM}} - u_{i,\mathrm{avg}}^{\mathrm{EQ}}\right) \\ &= \mathscr{B}(\mathbf{u}^{\mathrm{LM}} - \mathbf{u}^{\mathrm{EQ}}, G_i^{\mathrm{LM}})\end{aligned} \tag{29}$$

If G_i^{EQ} corresponds to $\mathscr{B}(G_i^{\mathrm{EQ}}, \mathbf{v}^{\mathrm{EQ}}) = v_{i,\mathrm{avg}}^{\mathrm{EQ}}$, with G_i^{EQ} and $\mathbf{v}^{\mathrm{EQ}}$ corresponding to the EQ3333 model, then we have $\mathscr{B}(\mathbf{u}^{\mathrm{LM}} - \mathbf{u}^{\mathrm{EQ}}, G_i^{\mathrm{EQ}}) = 0$. Hence

$$\begin{aligned}u_{i,\mathrm{avg}}^{\mathrm{LM}} - u_{i,\mathrm{avg}}^{\mathrm{EQ}} &= \mathscr{B}\left(\mathbf{u}^{\mathrm{LM}} - \mathbf{u}^{\mathrm{EQ}}, G_i^{\mathrm{LM}} - G_i^{\mathrm{EQ}}\right) \\ &= \sum_{\tau \in P_{\bar{v}}} \mathscr{B}\left(\mathbf{u}^{\mathrm{LM}} - \mathbf{u}^{\mathrm{EQ}}, G_i^{\mathrm{LM}} - G_i^{\mathrm{EQ}}\right) \\ &\quad + \sum_{\tau \in P_{\bar{v}'}} \mathscr{B}(\mathbf{u}^{\mathrm{LM}} - \mathbf{u}^{\mathrm{EQ}}, G_i^{\mathrm{LM}} - G_i^{\mathrm{EQ}}) \\ &\leqslant \sum_{\tau \in P_{\bar{v}}} \|\mathbf{u}^{\mathrm{LM}} - \mathbf{u}^{\mathrm{EQ}}\|_\tau \|G_i^{\mathrm{LM}} - G_i^{\mathrm{EQ}}\|_\tau \\ &\quad + \sum_{\tau \in P_{\bar{v}'}} \|\mathbf{u}^{\mathrm{LM}} - \mathbf{u}^{\mathrm{EQ}}\|_\tau \|G_i^{\mathrm{LM}} - G_i^{\mathrm{EQ}}\|_\tau\end{aligned} \tag{30}$$

where $P_{\bar{v}}$ is a small (one layer) neighborhood of region of interest $\bar{v}$. It is now obvious that if the errors $\|\mathbf{u}^{\mathrm{LM}} - \mathbf{u}^{\mathrm{EQ}}\|_\tau$, $\|G_i^{\mathrm{LM}} - G_i^{\mathrm{EQ}}\|_\tau$ are large in some elements, then they contribute significantly to $u_{i,\mathrm{avg}}^{\mathrm{LM}} - u_{i,\mathrm{avg}}^{\mathrm{EQ}}$. In this case, the significant contribution comes from the region near the singular edge. This is further substantiated by using the RR-U model. Here, the LM model is used in

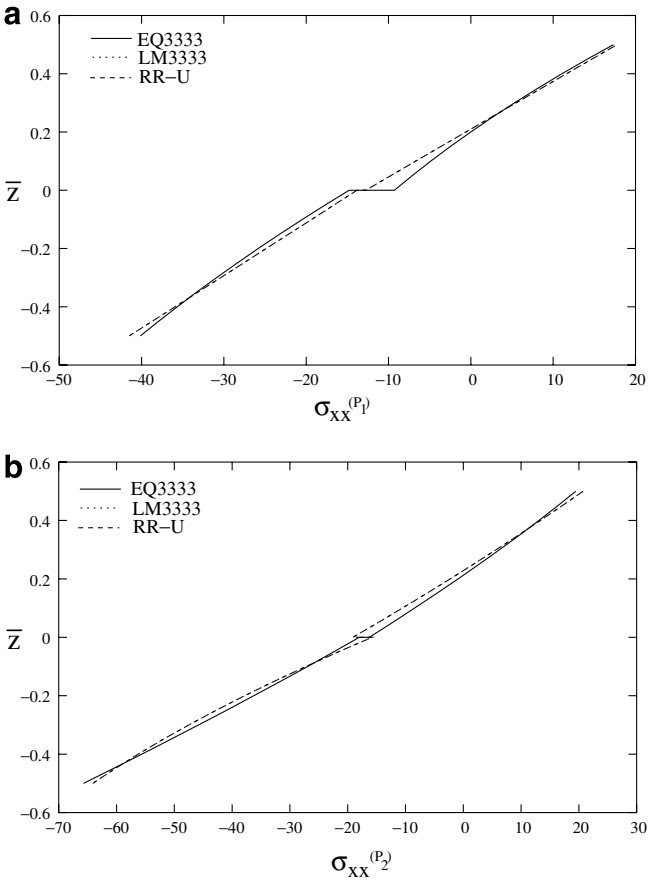

Fig. 21. In-plane stress for beam without sublayers. (a) At point 1 and (b) at point 2.

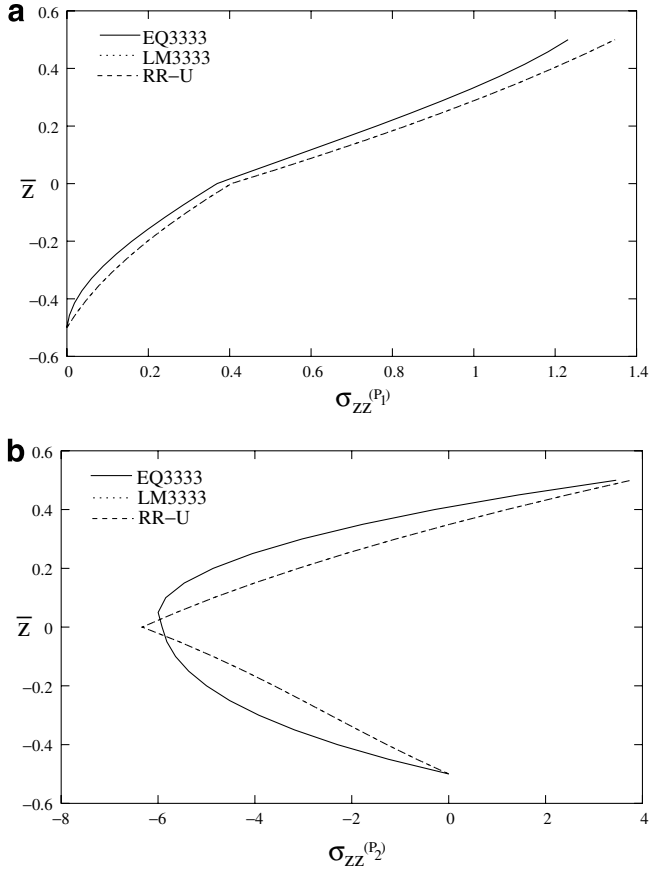

Fig. 22. Transverse normal stress (equilibrium based postprocessing) for beam without sublayers. (a) At point 1 and (b) at point 2.

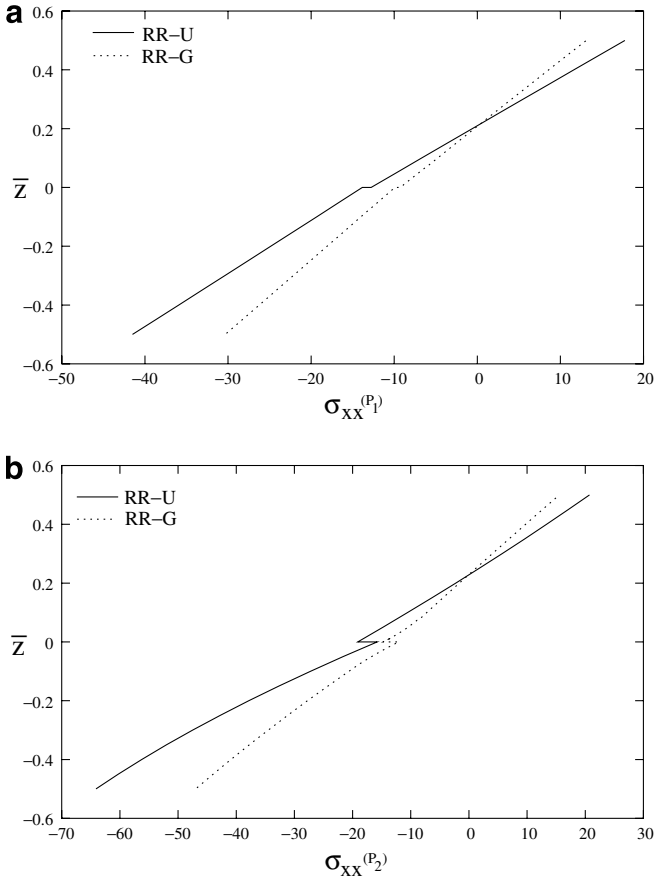

Fig. 23. In-plane stress for beam with graded sublayers. (a) At point 1 and (b) at point 2.

the vicinity of the singular edge only. Here, the error $\|\mathbf{u}^{\mathrm{LM}} - \mathbf{u}^{\mathrm{RR\text{-}U}}\|_{\tau}$, $\|G_i^{\mathrm{LM}} - G_i^{\mathrm{RR\text{-}U}}\|_{\tau}$ is small for the elements near the singular edge. Hence, the displacement $u_i^{\mathrm{RR\text{-}U}}$ is very close to u_i^{LM} everywhere, including the boundary. This clearly demonstrates that the augmentation of the model has to be done in the non-smooth regions (which, in this case, is far from the region of interest) also, in order to get good local solutions. In all the earlier examples, the solution was smooth everywhere in the domain and model pollution effect was negligible. This simple problem also highlights one of the major drawbacks of ad-hoc global–local computations, where the model and mesh are suitably refined only in the vicinity of the region of interest (for details see [39,40]). Based on the analysis given above, an a posteriori modeling error estimator (for the quantity of interest) can be developed. This can be used, along with the region-by-region approach outlined in this paper, to develop an adaptive modeling error control algorithm. The modeling error estimators will be discussed in a subsequent paper.

The need for use of sublaminae in the vicinity of regions where the solution is non-smooth, will be further demonstrated through a study of the stress obtained at points $P_1(40, 5, \bar{z})$ and $P_2(60, 5, \bar{z})$, shown in Fig. 19(a).

7.3.2. Stress analysis

The through thickness variation of the stress components is given for two points P_1 and P_2. The in-plane stress σ_{xx} obtained using EQ3333, LM3333 and RR-U model is shown in Fig. 21. The equilibrium based postprocessed stress σ_{zz} obtained with EQ3333, LM3333 and RR-U model is shown in Fig. 22. From the figures we observe that:

1. All the stress components, obtained by the EQ3333 models, are quantitatively and qualitatively different from those obtained by the LM3333 model.
2. The RR-U strategy gives stress values that are very close to those obtained by the LM3333 model.

Here, the LM3333 model was our benchmark. The pointwise stresses due to the RR-U scheme are very close to those obtained by the LM3333 model.

Since the exact solution of this problem is expected to not be smooth in the vicinity of the singular edge, for a better approximation graded sublaminae were used in the RR-G model in the vicinity of the singular edge. The RR-G strategy is compared with the RR-U strategy in Figs. 23 and 24. From the figures we observe that the RR-U and RR-G strategy give in-plane and postprocessed stresses

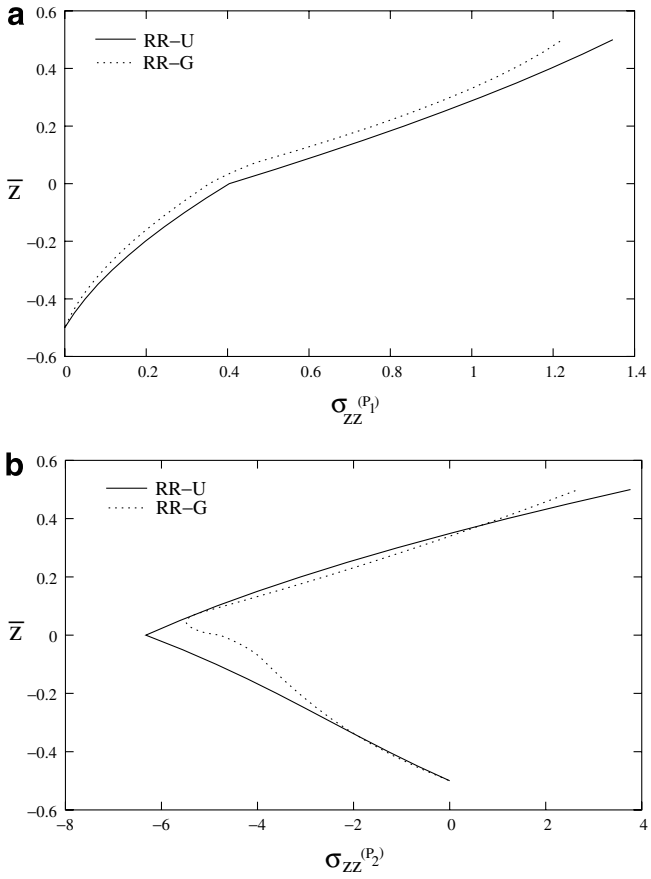

Fig. 24. Transverse normal stress (equilibrium based postprocessing) for beam with graded sublayers. (a) At point 1 and (b) at point 2.

Table 10
Number of unknowns for multimaterial beam problem

Model	Throughout EQ3333	Throughout LM3333	RR3333-U	RR3333-G
Unknowns	28,812	50,421	38,955	92,757

very close (overlapping lines). The example clearly demonstrates the ineffectiveness of the EQ models. It further demonstrates the effectiveness of the RR-U and RR-G strategies. Note that with the RR-G strategy, the value of σ_{zz} at the top reaches closer to the exact value of 1. Further graded sublaminae and mesh has to be used in the vicinity of singular edge to get the pointwise value of the transverse stress components at the given point more accurately. This can be achieved by using a suitable a posteriori error estimator for modeling error, along with the RR-G strategy.

In Table 10, the number of unknowns for each of the solution strategies, is given. From the table it is clear that the RR-U or RR-G strategy leads to significant savings in the computational cost as compared to the LM model.

8. Conclusions

In this study, we presented some families of plate models. A study of their local quality was carried out. A new region-by-region modeling approach was introduced. Below we give some of the major conclusions that can be drawn from this study:

1. The equivalent, intermediate and layerwise models employed in this study give accurate in-plane stresses, as has been extensively reported in the literature for such classes of models. These models display the expected accuracy for transverse stress components also.
2. The equilibrium approach for computing transverse stresses is accurate for all the models, for symmetric and antisymmetric laminates.
3. The equivalent, intermediate and layerwise models fail in the presence of singular vertices, singular edges and material transitions. In all these cases the solution is locally non-smooth and is strongly three-dimensional in nature. This requires the layerwise models to be augmented locally by using graded sublayers, along with a geometrically graded in-plane mesh.
4. The concept of region-by-region modeling, with different models in different regions of the domain has been proposed and implemented.
5. Generally, using LM model in a one-layer neighborhood of region of interest is enough. Outside this region, a low order equivalent model can be used, leading to significant reduction in computational cost.
6. The region-by-region approach allows for augmentation of the model in regions where the three-dimensional effects are very pronounced. The strategy allows the user to put the layerwise model, along with graded sublayers in the vicinity of the region where the solution is non-smooth. This leads to better local resolution of the three-dimensional effects and hence a more accurate evaluation of any pointwise quantity of interest.
7. The proposed modeling strategy, along with robust a posteriori discretization and modeling error estimators, can be naturally used in a general adaptive finite element analysis for any plate configuration.

References

[1] Babuska I, Szabó BA, Actis RL. Hierarchic models for laminated composites. Int J Numer Methods Eng 1992;33:503–35.
[2] Actis RL, Szabó BA, Schwab C. Hierarchic models for laminated plates and shells. Comput Methods Appl Mech Eng 1999;172:79–107.
[3] Lo KH, Christensen RM, Wu EM. A higher-order theory of plate deformation. Part 2: laminated plates. J Appl Mech, Trans ASME 1977;44:669–76.
[4] Reddy JN. A simple higher order theory for laminated composite plates. J Appl Mech, Trans ASME 1984;51:745–52.
[5] Carrera E. Evaluations of layerwise mixed theories for laminated plates analysis. AIAA J 1998;36:830–9.
[6] Lage RG, Soares CMM, Soares CAM, Reddy JN. Analysis of adaptive plate structures by mixed layerwise finite elements. Compos Struct 2004;66:261–8.
[7] Carrera E. An assessment of mixed and classical theories on global and local response of multilayered orthotropic plates. Compos Struct 2000;50:183–98.

[8] Carrera E. Developments, ideas, and evaluations based upon Reissner's Mixed Variational Theorem in the modeling of multilayered plates and shells. Appl Mech Rev 2001;54(4):301–29.
[9] Carrera E. Historical review of zig-zag theories for multilayered plate and shells. Appl Mech Rev 2003;56(3):287–308.
[10] Toledano A, Murakami H. A composite plate theory for arbitrary laminate configurations. J Appl Mech, Trans ASME 1987;54:181–9.
[11] Mohite PM, Upadhyay CS. Accurate computation of critical local quantities in composite laminated plates under transverse loading. Comput Struct 2006;84:657–75.
[12] Mohite PM, Upadhyay CS. Reliable computational of local quantities of interest in composite laminated plates. In: 46th AIAA/ASME/ASCE/AHS/ASC structures, structural dynamics and material conference Texas, Austin, 18–21 April, 2005.
[13] Kuhlmann G, Rolfes R. A hierarchic 3D finite element for laminated composite. Int J Numer Methods Eng 2004;61:96–116.
[14] Carrera E. Theories and finite elements for multilayered, anisotropic, composite plates and shells. Arch Comput Methods Eng 2002;9(2):87–140.
[15] Ahmed NU, Basu PK. Higher-order finite element modeling of laminated composite plates. Int J Numer Methods Eng 1994;37:123–9.
[16] Di Sciuva M. Development of an anisotropic, multilayered, shear-deformable rectangular plate element. Comput Struct 1985;21:789–96.
[17] Bhaskar K, Varden TK. Refinement of higher-order laminated plate theories. AIAA J 1989;27(12):1830–1.
[18] Sheikh NA, Upadhyay CS, Venkatesan C. Electro-elastic analysis and layer-by-layer modeling of a smart beam. AIAA J 2005;43(12):2606–16.
[19] Garção JES, Soares CMM, Soares CAM, Reddy JN. Analysis of laminated adaptive structures using layerwise finite elements. Comput Struct 2004;82:1939–59.
[20] Mitchell JA, Reddy JN. A hierarchical iterative procedure for the analysis of composite laminates. Comput Methods Appl Mech Eng 2000;181:237–60.
[21] Reddy JN. Mechanics of laminated composite plates and shells. 2nd ed. Boca Raton, USA: CRC Press; 2004.
[22] Arnold DN, Falk RS. A uniformly accurate finite element method for the Reissner–Mindlin plate. SIAM J Numer Anal 1990;26(6):1726–90.
[23] Babuska I, Li L. The *h–p* version of the finite element method in the plate modelling problem. Commun Appl Numer Methods 1992;8:17–26.
[24] Babuska I, Schwab C. A posteriori error estimation for hierarchic models of elliptic boundary value problems on thin domains. SIAM J Numer Anal 1996;23(1):221–46.
[25] Babuska I, Suri M. The *p* and *h–p* versions of the finite element method, basic principles and properties. SIAM Rev 1994;36:578–632.
[26] Schwab C, Suri M, Xenophontos C. The *hp* finite element method for problems in mechanics with boundary layers. Seminar för Angewandte Mathematik Eidgenössische Technische Hochschule CH-8092 Zörich Switzerland Research Report No. 96-20, October 1996.
[27] Hakula H, Leino Y, Pitkäranta J. Scale resolution, locking, and high-order finite element modelling of shells. Comput Methods Appl Mech Eng 1996;133:157–82.
[28] Dhia HB, Rateau G. The Arlequin method as a flexible engineering design tool. Int J Numer Methods Eng 2005;62:1442–62.
[29] Fish J. The *s*-version of the finite element method. Comput Struct 1992;43(3):539–47.
[30] Reddy JN, Robbins D. Theories and computational models for composite laminates. Appl Mech Rev 1994(47):147–69.
[31] Babuska I, Stroubulis S, Upadhyay CS, Gangaraj SK. A posteriori estimation and adaptive control of the pollution error in the *h* version of the finite element method. Int J Numer Methods Eng 1995;38:4207–35.
[32] Demkowicz L, Oden JT, Rachowicz W, Hardy O. Towards a universal *h–p* adaptive finite element strategy, part 1 constrained approximation and data structure. Comput Methods Appl Mech Eng 1989;77:79–112.
[33] Stein E, Rust W, Ohnimus S. *h* and *d* adaptive FE methods for two dimensional structural problems including post-buckling of shells. Comput Methods Appl Mech Eng 1992;101:315–53.
[34] Schwab C. A-posteriori modeling error estimation for hierarchic plate model. Numer Math 1996;74:221–59.
[35] Pagano NJ, Hatfield SJ. Elastic behavior of multilyered bidirectional composites. AIAA J 1972;10:931–3.
[36] Pagano NJ. Influence of shear coupling in cylindrical bending of anisotropic laminates. J Compos Mater 1970;4:330–43.
[37] Tsai SW, Wu EM. A general theory of strength for anisotropic materials. J Compos Mater 1971;5:55–80.
[38] Reddy YSN, Reddy JN. Linear and non-linear failure analysis of composite laminates with transverse shear. Compos Sci Technol 1992;44:227–55.
[39] Mohite PM, Upadhyay CS. Local quality of smoothening based a-posteriori error estimators for laminated plates under transverse loading. Comput Struct 2002;80(18-19):1477–88.
[40] Mohite PM, Upadhyay CS. Focussed adaptivity for laminated plates. Comput Struct 2003;81:287–98.